Nuclear Operating Company

South Texas Project Electric Generating Station 4000 Avenue F – Suite A Bay City, Texas 77414

August 12, 2008
ABR-AE-08000061

U. S. Nuclear Regulatory Commission
Attention: Document Control Desk
One White Flint North
11555 Rockville Pike
Rockville MD 20852-2738

South Texas Project
Units 3 and 4
Docket Nos. 52-012 and 52-013
Response to Requests for Additional Information

Attached are responses to NRC staff questions included in Request for Additional Information (RAI) letter numbers 31, 34, 39, 40, 49, 50 and 52 related to Combined License Application (COLA) Part 2, Tier 2 Sections 2.4S and 2.5S. This submittal includes responses to the following Question numbers:

02.04.02-3	02.04.13-1	02.05.01-12	02.05.04-9
02.04.05-7	02.04.13-4	02.05.01-13	02.05.04-10
02.04.12-5	02.04.13-8	02.05.02-11	02.05.04-11
02.04.12-17	02.04.13-9		

When a change to the COLA is indicated by a question response, the change will be incorporated into the next routine revision of the COLA following NRC acceptance of the question response.

There are no commitments in this letter.

If you have any questions regarding the attached responses, please contact me at (361) 972-4626, or Bill Mookhoek at (361)-972-7274.

D079
NRO

STI: 32344830

I declare under penalty of perjury that the foregoing is true and correct.

Executed on August 12, 2008

Gregory T. Gibson
Manager, Regulatory Affairs
South Texas Project Units 3 & 4

sab

Attachments:
1. Question 02.04.02-3
2. Question 02.04.05-7
3. Question 02.04.12-5
4. Question 02.04.12-17
5. Question 02.04.13-1
6. Question 02.04.13-4
7. Question 02.04.13-8
8. Question 02.04.13-9
9. Question 02.05.01-12
10. Question 02.05.01-13
11. Question 02.05.02-11
12. Question 02.05.04-9
13. Question 02.05.04-10
14. Question 02.05.04-11

cc: w/o attachment except*
(paper copy)

Director, Office of New Reactors
U. S. Nuclear Regulatory Commission
One White Flint North
11555 Rockville Pike
Rockville, MD 20852-2738

Regional Administrator, Region IV
U. S. Nuclear Regulatory Commission
611 Ryan Plaza Drive, Suite 400
Arlington, Texas 76011-8064

Richard A. Ratliff
Bureau of Radiation Control
Texas Department of State Health Services
1100 West 49th Street
Austin, TX 78756-3189

C. M. Canady
City of Austin
Electric Utility Department
721 Barton Springs Road
Austin, TX 78704

*Steven P. Frantz, Esquire
A. H. Gutterman, Esquire
Morgan, Lewis & Bockius LLP
1111 Pennsylvania Ave. NW
Washington D.C. 20004

*George F. Wunder
Two White Flint North
11545 Rockville Pike
Rockville, MD 20852

*Raj Anand
Two White Flint North
11545 Rockville Pike
Rockville, MD 20852

(electronic copy)

*George F. Wunder
*Raj Anand
Loren R. Plisco
U. S. Nuclear Regulatory Commission

Brad Porlier
Steve Winn
Eddy Daniels
NRG South Texas 3/4 LLC

Jon C. Wood, Esquire
Cox Smith Matthews

J. J. Nesrsta
R. K. Temple
Kevin Pollo
L. D. Blaylock
CPS Energy

RAI 02.04.02-3:

QUESTION:

Provide a discussion of (A) flood magnitude and timing; (B) the effect on water levels in the power block area; and, (C) the effect of the 34 ft MSL constant water level boundary condition in HEC-RAS simulation, if FM 521 were not to act like a barrier and flood runoff from North 1 and 2 subbasins were not lagged significantly. Provide justification for using a 6-hr PMP, rather than using a shorter duration and more intense PMP value, to obtain a peak PMF water level in the power block area. Specify in the FSAR, at which spot within the power block area, the peak flooding level was simulated.

RESPONSE:

In order to provide clarity, the response to this question is provided in three parts:

RAI Part 1: Provide a discussion of (A) flood magnitude and timing; (B) the effect on water levels in the power block area; and, (C) the effect of the 34 ft MSL constant water level boundary condition in HEC-RAS simulation, if FM 521 were not to act like a barrier and flood runoff from North 1 and 2 subbasins were not lagged significantly.

RAI Part 1 Response:

In the analysis of local probable maximum precipitation (LPMP) flooding, presented in Revision 0 of FSAR 2.4S.2 (also referred to as the COLA base case in this response), highway FM 521 was modeled as a drainage divide. It separated subbasins North1 and North2, as defined in Revision 0 of FSAR Figure 2.4S.2-5, in the north and west sides of the STP 3 and 4 site from the rest of the contributing drainage area of the Main Drainage Channel (MDC) (Revision 0 FSAR Figure 2.4S.2-4). Flood flow from North1 and North2 was postulated to pass through the culvert crossing of FM521 at Little Robins Slough (LRS), and also spill over the road crest towards LRS when the flood level was high. FM 521 was modeled as drainage divide that backs up flood flow from North1 and North2 because it has a road crest elevation of 32 ft NGVD29, which is about 4 ft higher than the surrounding natural ground elevation of approximately 28 ft NGVD29. If FM 521 were not to act like a barrier, flood flow from North1 and North2 towards LRS and MDC would be not restricted, and would potentially have a smaller lag behind the flood flow from other contributing subbasins. Two new modeling scenarios, each representing a different bounding level of effectiveness of FM 521 as a flow barrier, are formulated to evaluate the impact of FM 521 on the LPMP flooding pattern as described below.

In Scenario 1, flood flow from North1 and North2 is assumed to discharge to LRS unimpeded. This is accomplished in the HEC-HMS flood routing model (Reference 1) by assigning a junction element, instead of a reservoir element as in the COLA base case, at the FM 521 crossing at LRS. The conceptual model for Scenario 1 as represented in HEC-HMS is shown on

Figure 1, while the scheme for the COLA base case presented in the FSAR is shown on Figure 2.4S.2-6 of Revision 0 of the FSAR.

In Scenario 2, FM 521 is assumed to be completely ineffective as a flow barrier and no longer constitutes a drainage divide between subbasins North1/North2 and North3. Flood flow from the northern subbasins North1, North2 and North3, now combined to form a bigger subbasin North1A, would discharge to MDC at its junction with LRS. The conceptual model of Scenario 2 as represented in HEC-HMS is shown on Figure 2.

The HEC-HMS modeling results of the two scenarios show that Scenario 1 produces a higher flood peak at the junction of LRS and MDC (model junction "Outflow") than Scenario 2 (at model junction "Outflow"). This is primarily a result of the longer time of concentration estimated for the larger subbasin North1A, which has a longer flow path. Consequently, the predicted flood hydrograph for Scenario 1 is used to estimate the maximum water level in the power block area by using the HEC-RAS model previously developed for the COLA base case.

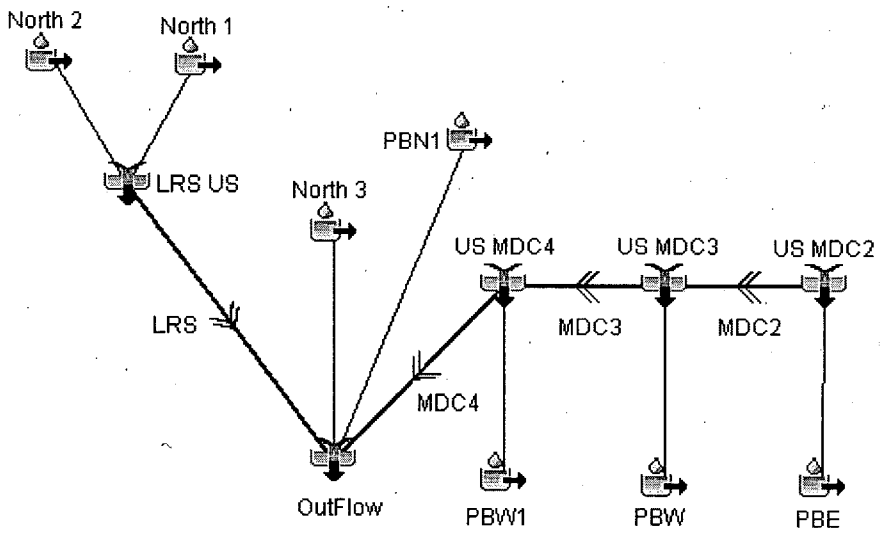

Figure 1 – HEC-HMS Hydrologic Diagram for Scenario 1

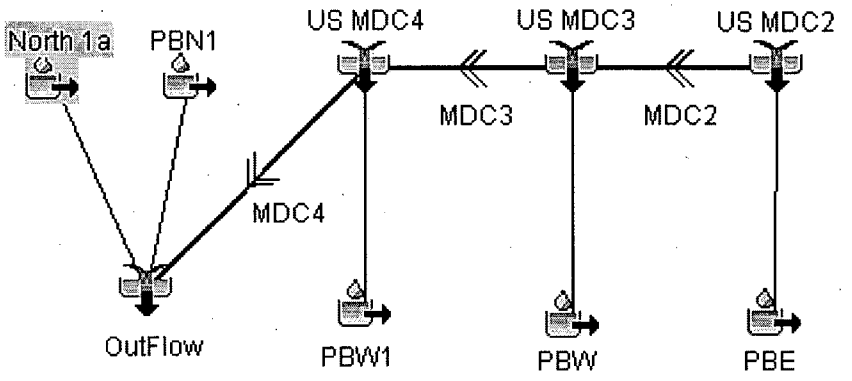

Figure 2 – HEC-HMS Hydrologic Diagram for Scenario 2

(A) Flood Magnitude and Timing

The HEC-HMS results for Scenario 1 show that the peak discharge from the northern subbasins (North1 and North2) that contributes to LRS (9,714.9 cfs) is higher and arrives earlier (5:25 hrs into the storm) than the peak discharge (7,690.3 cfs) and arrival time (6:25 hrs into the storm) from the COLA base case. For Scenario 1, the predicted peak discharge at model junction Outflow is 11,459.6 cfs, which is about 16% higher than the peak discharge of 9852.0 cfs from the COLA base case simulation. The arrival times of the peaks are nearly the same, 3:35 hrs and 3:40 hrs into the storm, respectively. The peak discharges and their arrival times at the subbasin outlets for the eastern subbasins (PBE, PBW, PBN1 and PBW1) remain unchanged. The predicted peak discharges and the corresponding flood peak arrival time for each subbasin are shown in Table 1. A time step of 5 min is used in the HEC-HMS model simulation.

(B) Effect on Water Levels in the Power Block Area

For water level estimation, the steady-flow routing option in HEC-RAS is used. As in the COLA base case simulation, the predicted flood hydrographs from the HEC-HMS model at each of the subbasin outlets and junction elements are used to establish the inflow at the corresponding model channel cross sections in the HEC-RAS model. Because the HEC-HMS flood hydrograph at Junction Outflow peaks at 3:40 hrs into the storm, the predicted flood discharges at Junction LRS US and at the outlet of subbasin North3 at 3:40 hrs are used to estimate the HEC-RAS inflow. However, for subbasins PBW, PBE, PBN1 and PBW1, the peaks of the predicted flood hydrographs are conservatively used, regardless of their peak arrival times. This conservative approach results in approximately 16% higher flow discharge (13,293.1 cfs) assigned to the downstream-most section (West Access Road) in the HEC-RAS model than the peak flow of 11459.6 cfs at junction Outflow predicted in the HEC-HMS model. A similar approach was used in the COLA base case simulation, where the peak flow at the downstream-most cross section was 11,080.4 cfs. The Scenario 1 peak discharge at the downstream-most cross section (13,293.1 cfs) is about 20% higher than the corresponding peak discharge used in the COLA

base case. The incremental and cumulative discharges at each HEC-RAS river cross section for Scenario 1 are shown in Table 2.

The maximum water level near the power block area is predicted to be 36.8 ft MSL for Scenario 1. This elevation is 0.2 ft higher than the flood elevation from the COLA base case. Although the peak discharge at the outflow location is increased by about 20% for Scenario 1 compared to that in COLA base case, the increase in the maximum flood elevation is only about 0.6%.

This maximum flood water level of 36.8 ft MSL occurs in the East Channel at the most-upstream river station (Cross Section or CS 1690), as well as at two cross sections on the East Channel near the Unit 3 reactor building, CS 1000 and CS 1200. The locations of the cross sections are shown on Figure 2.4S.2-7 of the Revision 0 of the FSAR.

It should be noted that the predicted increase in the peak water level in the power block for Scenario 1 is the result of using conservative assumptions in establishing the conceptual model that do not reflect the realistic flood routing characteristics in the contributing drainage area. For instance, Scenario 1, which represents a partial breach of FM 521 near the LRS crossing, does not account for the attenuation of the flood peaks from the northern subbasins due to the backwater effects at the narrow FM 521 breach. Similarly, Scenario 2, which represents complete failure of FM 521, does not account for the reduction of flood flow as a portion of the runoff from the northern subbasins would be diverted away from the MDC and LRS without FM 521.

(C) Effect of the 34 ft MSL Constant Water Level Boundary Condition in HEC-RAS Simulation

The sensitivity of the constant water level downstream boundary condition on the upstream water levels is discussed in Revision 0 of FSAR Subsection 2.4S.2.3.4. It indicates that the critical flow condition exists at the West Access Road crossing when the water level downstream is at 34 ft MSL or below. The general topography of the areas shows that there would only be minor changes to the drainage divide and flood flow patterns downstream of the West Access Road crossing in the hypothetical event that FM 521 would not act as a barrier. Therefore, the 34 ft MSL downstream boundary condition used in the COLA base case and Scenario 1 would still be valid.

No COLA revision is required as a result of this Part 1 response.

Table 1 – STP 3 & 4 Site PMP Peak Discharges for Scenario 1

Hydrologic Element	Drainage Area (mi^2)	Peak Discharge (cfs)	Time of Peak	Runoff Volume (in)
LRS	1.764	9707.1	26Jul2007, 05:35	31.68
LRS US	1.764	9714.9	26Jul2007, 05:25	31.68
MDC2	0.089	1428.7	26Jul2007, 03:30	31.68
MDC3	0.224	3588.4	26Jul2007, 03:35	31.68
MDC4	0.273	3937.5	26Jul2007, 03:35	31.68
North 1	1.466	7971.5	26Jul2007, 05:30	31.68
North 2	0.298	1773.1	26Jul2007, 05:15	31.68
North 3	0.177	1457.3	26Jul2007, 04:25	31.68
OutFlow	2.533	**11459.6**	26Jul2007, 03:40	31.68
PBE	0.089	1443.3	26Jul2007, 03:25	31.68
PBN1	0.319	4243.8	26Jul2007, 03:35	31.68
PBW	0.135	2304.4	26Jul2007, 03:25	31.68
PBW1	0.049	1367.7	26Jul2007, 03:10	31.68
US MDC2	0.089	1443.3	26Jul2007, 03:25	31.68
US MDC3	0.224	3635.2	26Jul2007, 03:25	31.68
US MDC4	0.273	3976.3	26Jul2007, 03:30	31.68

Table 2 – HEC-RAS Inflow Discharges for Different Cross Sections (River Stations)

Channel	Reach	River Station	Downstream Reach Length (ft)	Contributing Subbasins	Incremental Inflow (cfs)	Model Discharge in HEC-RAS (cfs)	Comments
EastChannel	EC-R1	1690	90	PBE	632.5	632.5	Upstream CS
EastChannel	EC-R1	1600	200		90.1	722.6	
EastChannel	EC-R1	1400	200		90.1	812.6	
EastChannel	EC-R1	1200	200		90.1	902.7	
EastChannel	EC-R1	1000	200		90.1	992.8	
EastChannel	EC-R1	0800	200		90.1	1082.9	
EastChannel	EC-R1	0600	200		90.1	1173.0	
EastChannel	EC-R1	0400	200		90.1	1263.1	
EastChannel	EC-R1	0200	100		90.1	1353.2	
EastChannel	EC-R1	0150	In-line Structure				
EastChannel	EC-R1	0050	0		90.1	1443.3	
LRS	LRS-R1	2200	200	North1, North2, North3[a]	3099.8	3099.8	From LRS US[a]
LRS	LRS-R1	2000	200		83.4	3183.2	
LRS	LRS-R1	1800	200		83.4	3266.6	
LRS	LRS-R1	1600	200		83.4	3350.0	
LRS	LRS-R1	1400	200		83.4	3433.4	
LRS	LRS-R1	1200	200		83.4	3516.9	
LRS	LRS-R1	1000	200		83.4	3600.3	
LRS	LRS-R1	0800	200		83.4	3683.7	
LRS	LRS-R1	0600	200		83.4	3767.1	
LRS	LRS-R1	0400	200		83.4	3850.5	
LRS	LRS-R1	0200	0		83.4	3933.9	

Table 2 – HEC-RAS Inflow Discharges for Different Cross Sections (River Stations) (continued)

Channel	Reach	River Station	Downstream Reach Length (ft)	Contributing Subbasins	Incremental Inflow (cfs)	Model Discharge in HEC-RAS (cfs)	Comments
MDC	MDC-R1	5380	100	PBE, PBW, PBN1, PBW1	1330.3	1330.3	Upstream CS
MDC	MDC-R2	5200	200		144.7	2918.3	EC flow added
MDC	MDC-R2	5000	200		144.7	3063.0	
MDC	MDC-R2	4800	200		144.7	3207.7	
MDC	MDC-R2	4600	200		144.7	3352.3	
MDC	MDC-R2	4400	200		144.7	3497.0	
MDC	MDC-R2	4200	200		144.7	3641.7	
MDC	MDC-R2	4000	200		144.7	3786.4	
MDC	MDC-R2	3800	200		144.7	3931.0	
MDC	MDC-R2	3600	200		144.7	4075.7	
MDC	MDC-R2	3400	0		144.7	4220.4	
MDC	MDC-R3	3200	200		144.7	6669.5	WC flow added
MDC	MDC-R3	3000	200		144.7	6814.1	
MDC	MDC-R3	2800	200		144.7	6958.8	
MDC	MDC-R3	2600	200		144.7	7103.5	
MDC	MDC-R3	2400	200		144.7	7248.2	
MDC	MDC-R3	2200	200		144.7	7392.8	
MDC	MDC-R3	2000	200		54.4	7447.3	
MDC	MDC-R3	1800	200		54.4	7501.7	
MDC	MDC-R3	1600	200		54.4	7556.1	
MDC	MDC-R3	1400	200		54.4	7610.5	

Table 2 – HEC-RAS Inflow Discharges for Different Cross Sections (River Stations) (continued)

Channel	Reach	River Station	Downstream Reach Length (ft)	Contributing Subbasins	Incremental Inflow (cfs)	Model Discharge in HEC-RAS (cfs)	Comments
MDC	MDC-R3	1200	200		54.4	9032.7	PBW1 flow added
MDC	MDC-R3	1000	200		54.4	9087.1	
MDC	MDC-R3	0800	200		54.4	9141.5	
MDC	MDC-R3	0600	0		54.4	9195.9	
MDC	MDC-R4	0400	200		54.4	13184.3	LRS flow added
MDC	MDC-R4	0200	100		54.4	13238.7	
MDC	MDC-R4	0050	In-line Structure				
MDC	MDC-R4	0000	0		54.4	13293.1	
WestChannel	WC-R1	1690	90	PBW	472.8	472.8	Upstream CS
WestChannel	WC-R1	1600	200		203.5	676.3	
WestChannel	WC-R1	1400	200		203.5	879.8	
WestChannel	WC-R1	1200	200		203.5	1083.4	
WestChannel	WC-R1	1000	200		203.5	1286.9	
WestChannel	WC-R1	0800	200		203.5	1490.4	
WestChannel	WC-R1	0600	200		203.5	1693.9	
WestChannel	WC-R1	0400	200		203.5	1897.4	
WestChannel	WC-R1	0200	100		203.5	2100.9	
WestChannel	WC-R1	0150	In-line Structure				
WestChannel	WC-R1	0050	0		203.5	2304.4	

[a] Inflow corresponding to 03:40 hrs into the storm

RAI Part 2: Provide justification for using a 6-hr PMP, rather than using a shorter duration and more intense PMP value, to obtain a peak PMF water level in the power block area.

RAI Part 2 Response:

The 6-hr PMP storm used as input to the HEC-HMS flood model is represented by PMP rainfall depths of 5 min, 15 min, 1 hr, 2 hrs, 3 hrs and 6 hrs durations as shown in Table 2.4S.2-4 of Revision 0 of FSAR. The effect of the more intense PMP values corresponding to shorter duration events, down to a 5-minute duration, on the water level in the power block area have been captured in the HEC-HMS and HEC-RAS analyses. Figure 3, which shows the distribution of precipitation intensities and resulting runoff hydrograph for the subbasin PBN1, is provided as an example.

No COLA revision is required as a result of this Part 2 response.

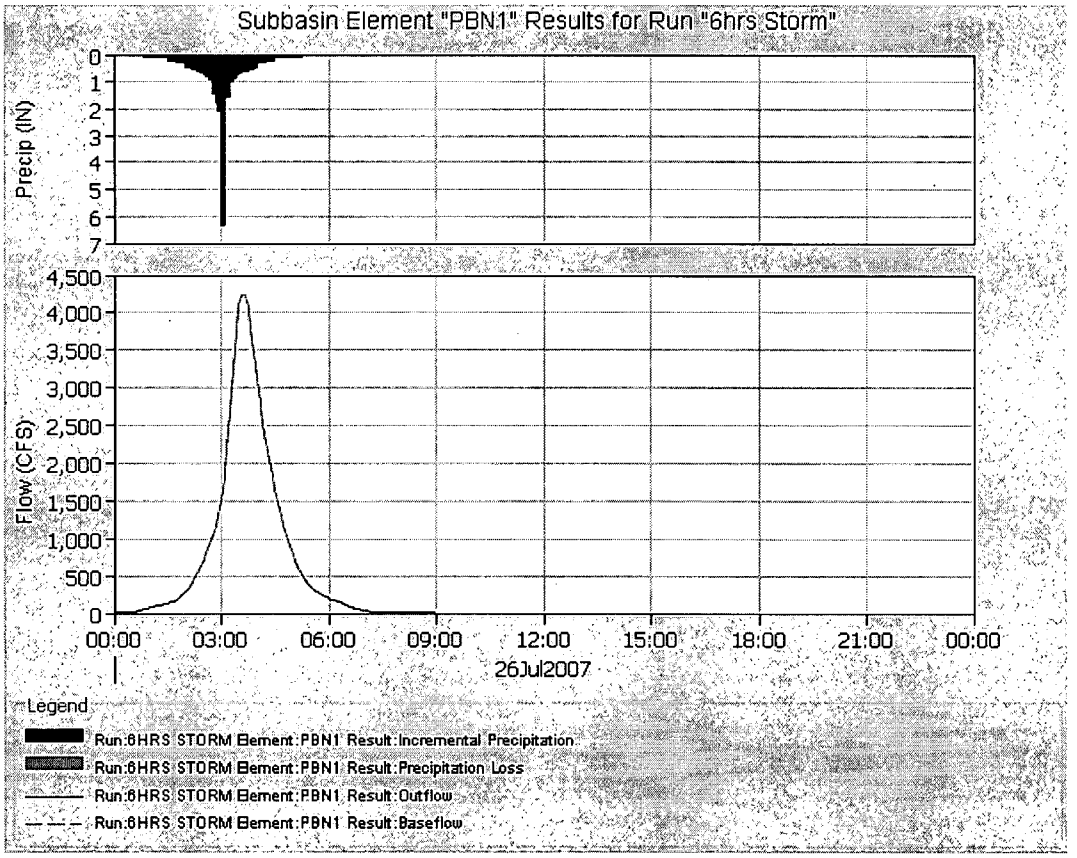

Figure 3 – Precipitation Distribution and Resulting Runoff for Subbasin PBN1

RAI Part 3: Specify in the FSAR, at which spot within the power block area, the peak flooding level was simulated.

RAI Part 3 Response:

The peak water level due to the local PMP storm event is computed on the East Channel within the protected area boundary. The maximum water level of 36.6 ft MSL occurs between river stations CS 1690 and CS 0050 with essentially a flat water surface elevation because of the back water effect from the MDC. The maximum water surface elevation would impact the safety-related reactor building and control building. In addition, the peak water levels along the entire West Channel are predicted to be at 36.4 ft MSL. Conservatively, it is assumed that the power block area with its safety related facilities are subject to the same peak flood level of 36.6 ft MSL during a local PMP event as stated in Revision 0 of FSAR Subsection 2.4S.2.3.5.

First paragraph of FSAR Section 2.4S.2.3.5 will be revised in the COLA as follows in response to Part 3 of this RAI:

> The HEC-RAS computer model simulation was used to estimate the maximum water surface elevation within the STP 3 & 4 power block area. Model simulation results showed that the maximum water surface elevation within the power block area was elevation 36.6 ft MSL. This elevation is conservatively assumed to affect the entire power block area of STP 3 & 4. This flooding elevation is higher than the power block grade elevation and the ground floor slab elevation of the safety-related SSCs. However, the local PMP water surface elevation is less than the flood elevation estimated from the postulated breach of the MCR embankment, which was estimated to be at elevation 47.6 ft MSL, as discussed in Subsection 2.4S.4. Flood protection measures for the safety-related SSCs against flooding due to the MCR embankment breach are sufficient to provide protection against flood elevation due to the local PMP storm event.

References:

1. U.S. Army Corps of Engineers, Hydrologic Engineering Center, HEC-HMS, Hydrologic Modeling System, Technical Reference Manual, March 2000

RAI 02.04.05-7:

QUESTION:

Provide an assessment of seismically induced seiche in the MCR.

RESPONSE:

Seiche effects in the MCR from atmospheric forcings (e.g., hurricanes) are referenced in Subsection 2.4S.5.2.6 and discussed in Subsection 2.4S.8.2.4. Seiche effects in the MCR from seismic forcings are not considered since the failure of the MCR is a bounding case and the design basis flood for STP 3 & 4. Failure of the MCR is discussed in Subsection 2.4S.4.

Section 2.4S.5.2.6 will be revised in the COLA as follows:

> Seiches are standing waves of relatively long period which occur in lakes, canals, bays, and on the open coast. Other than the Gulf of Mexico and Matagorda Bay, there are no large bodies of water in the immediate vicinity of the site, and seiche has not been considered as the controlling influence for these bodies of water. Other than for floods on the Colorado River, the hurricane storm surge is the dominant factor responsible for coastal area flooding. Therefore, the flooding at the site due to seiche effects from seismic or atmospheric external forcing mechanisms is considered insignificant in comparison to the water level at STP 3 & 4 resulting from the failure of the MCR. Failure of the MCR is discussed in Section 2.4S.4. Seiche effects ~~of~~in the MCR due to atmospheric mechanisms are discussed in Subsection 2.4S.8.2.4.

RAI 02.04.12-5:

QUESTION:

Provide detailed surface maps for top and bottom elevations of both Upper and Lower Shallow Aquifers as they are needed to better understand and predict on-site groundwater flow and pathways. Figure 2.4S.12-10 shows many piezometric wells around Units 1 and 2, but it is not clear whether the water level data from all the wells were used for the water level contour maps in Figure 2.4S.12-19. Please clarify.

RESPONSE:

The requested maps are attached. The maps are a geostatistical interpretation of available data representing the top and bottom elevations of the Upper Shallow Aquifer (Geotechnical Stratum C from FSAR 2.5S.4) and Lower Shallow Aquifer (Geotechnical Strata E and H from FSAR 2.5S.4). The tension-spline method in ESRI ArcGIS software was used to contour the available data. The data are from the Units 1 & 2 UFSAR (reference) and the STP Units 3 & 4 geotechnical evaluation.

The Lower Shallow Aquifer includes two sand units (Geotechnical Strata E and H) separated in places by a discontinuous clay unit (Geotechnical Stratum F from FSAR 2.5S.4). Where encountered in borings, this clay unit has been observed with a thickness that can range from about 0.7 feet to about 61.5 feet with an average of about 20 feet. However, the encountered thickness at most borings is between about 10 to 30 feet. (It should be noted several borings did not fully penetrate the unit.)

The water level contour maps in Figure 2.4S.12-19 used the data from the observation wells drilled during the 2006 - 2007 subsurface investigation for Units 3 & 4 (the "Units 3 & 4 wells"), because this was the only relevant data available for the two dates represented in that figure. The other piezometers shown in Figure 2.4S.12-10 were installed more than 20 years ago. Most of these piezometers no longer exist or relevant construction details are no longer available. The most recent data available from these piezometers are from May 1, 2006. The earliest data available for the "Units 3 & 4 wells" are from December 28, 2006 (Table 2.4S.12-7). These two data sets are not contemporaneous and, as a result, cannot be combined to prepare contour maps such as those in Figure 2.4S.12-19. Plans are underway to install additional observation wells at the STP site to obtain hydrogeologic information in the vicinity of Kelly Lake and to reduce the uncertainty associated with the groundwater flow paths near the MCR and site boundary.

No COLA revision is required as a result of this RAI response.

Reference:

STPEGS UFSAR Section 2.5.A-1, Appendix 2.5.A, Foundation Verification, Revision 13.

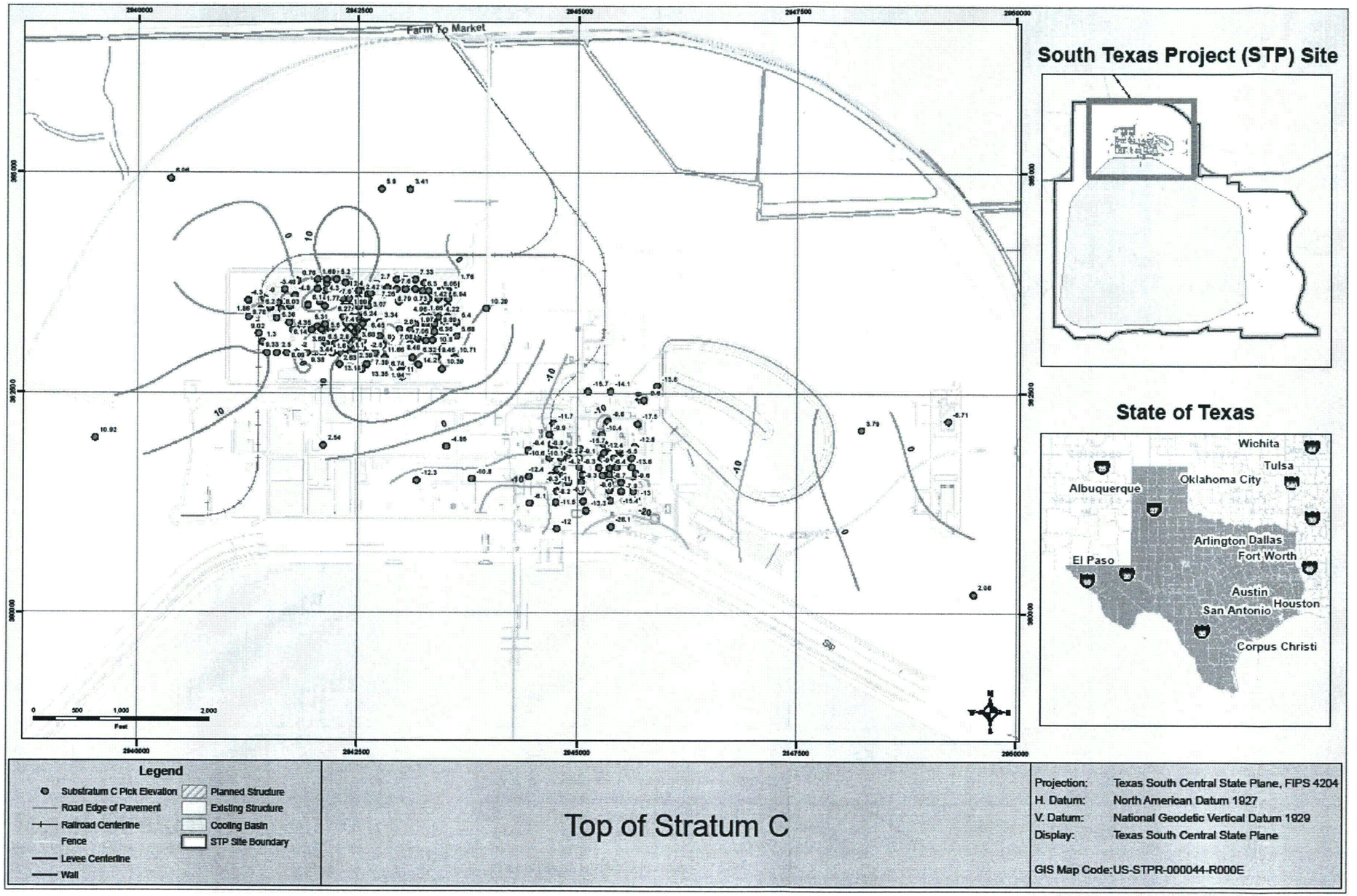

South Texas Project (STP) Site

State of Texas

Legend

- Substratum C Pick Elevation
- Road Edge of Pavement
- Railroad Centerline
- Fence
- Levee Centerline
- Wall
- Planned Structure
- Existing Structure
- Cooling Basin
- STP Site Boundary

Top of Stratum C

Projection: Texas South Central State Plane, FIPS 4204
H. Datum: North American Datum 1927
V. Datum: National Geodetic Vertical Datum 1929
Display: Texas South Central State Plane

GIS Map Code:US-STPR-000044-R000E

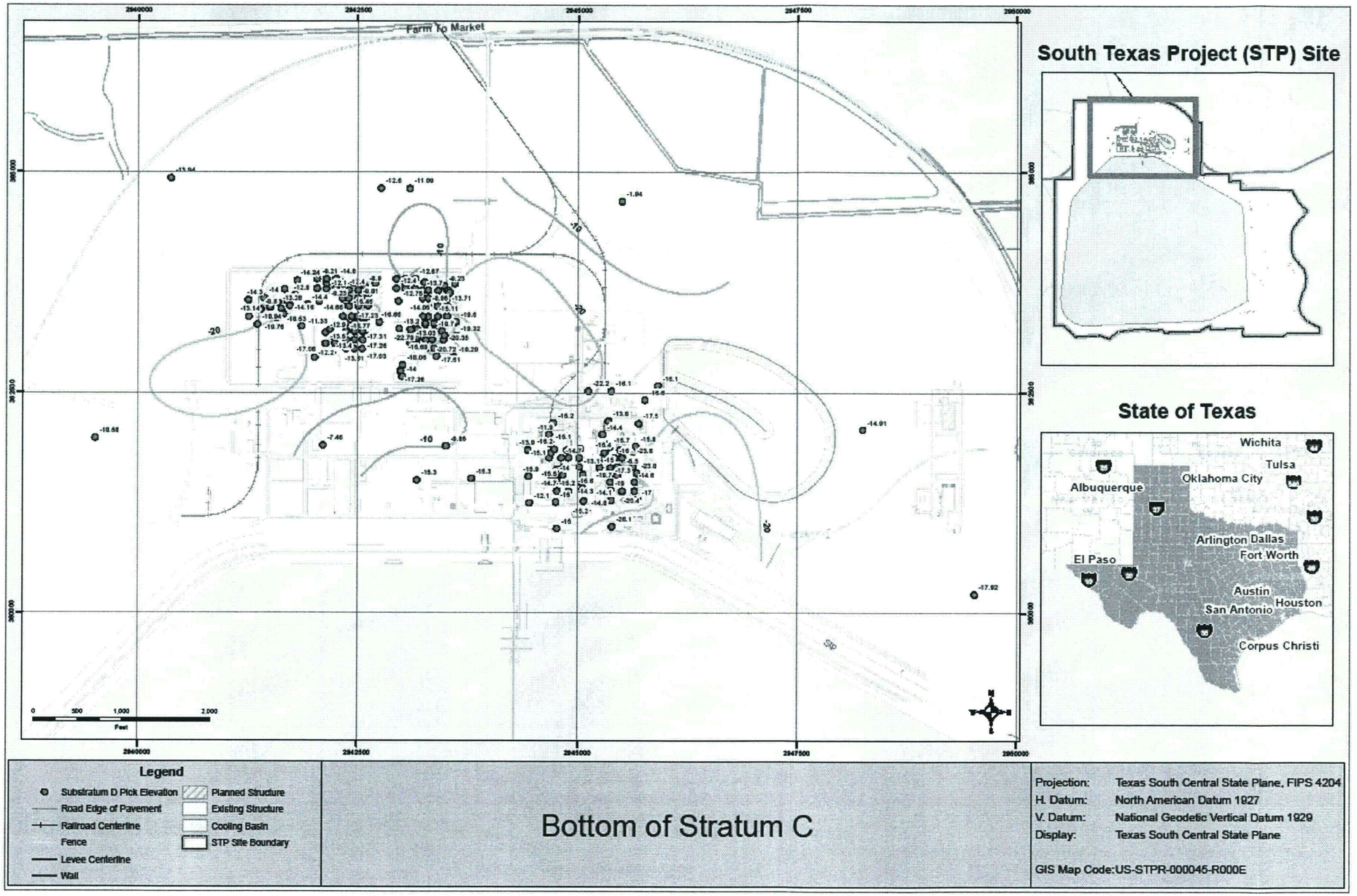
Farm to Market
South Texas Project (STP) Site
State of Texas
Wichita
Tulsa
Albuquerque
Oklahoma City
Arlington
Dallas
Fort Worth
El Paso
Austin
San Antonio
Houston
Corpus Christi
0 500 1,000 2,000
Feet
Legend
Substratum D Pick Elevation
Road Edge of Pavement
Railroad Centerline
Fence
Levee Centerline
Wall
Planned Structure
Existing Structure
Cooling Basin
STP Site Boundary
Bottom of Stratum C
Projection: Texas South Central State Plane, FIPS 4204
H. Datum: North American Datum 1927
V. Datum: National Geodetic Vertical Datum 1929
Display: Texas South Central State Plane
GIS Map Code:US-STPR-000045-R000E

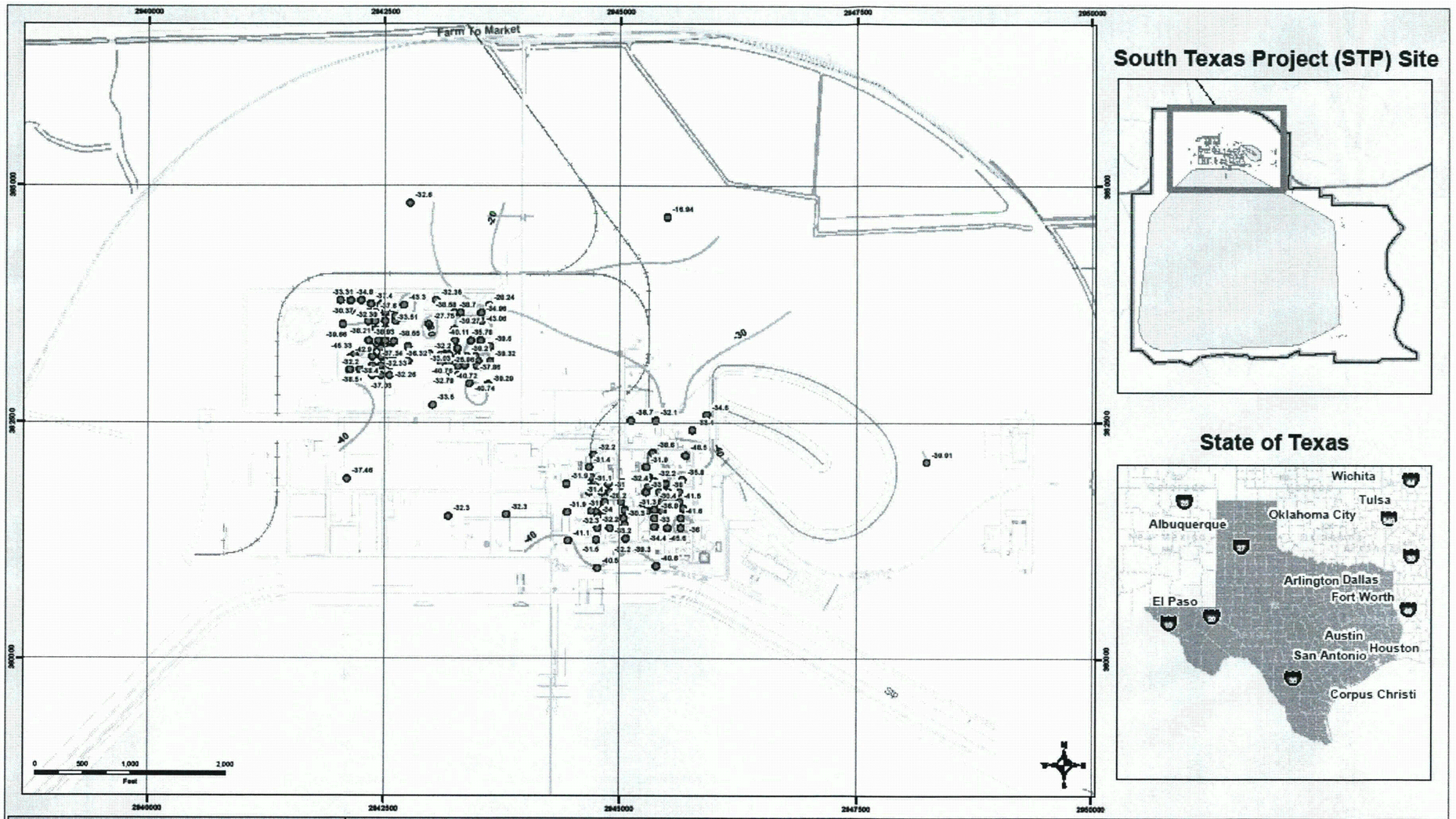
Farm To Market
2940000
2942500
2945000
2947500
2950000
392500
390000
387500
0
500
1,000
2,000
Feet
N
South Texas Project (STP) Site
State of Texas
Wichita
Tulsa
Albuquerque
Oklahoma City
Arlington
Dallas
Fort Worth
El Paso
Austin
San Antonio
Houston
Corpus Christi
Legend
Substratum E Pick Elevation
Road Edge of Pavement
Railroad Centerline
Fence
Levee Centerline
Wall
Planned Structure
Existing Structure
Cooling Basin
STP Site Boundary
Top of Stratum E
Projection: Texas South Central State Plane, FIPS 4204
H. Datum: North American Datum 1927
V. Datum: National Geodetic Vertical Datum 1929
Display: Texas South Central State Plane
GIS Map Code:US-STPR-000046-R000E

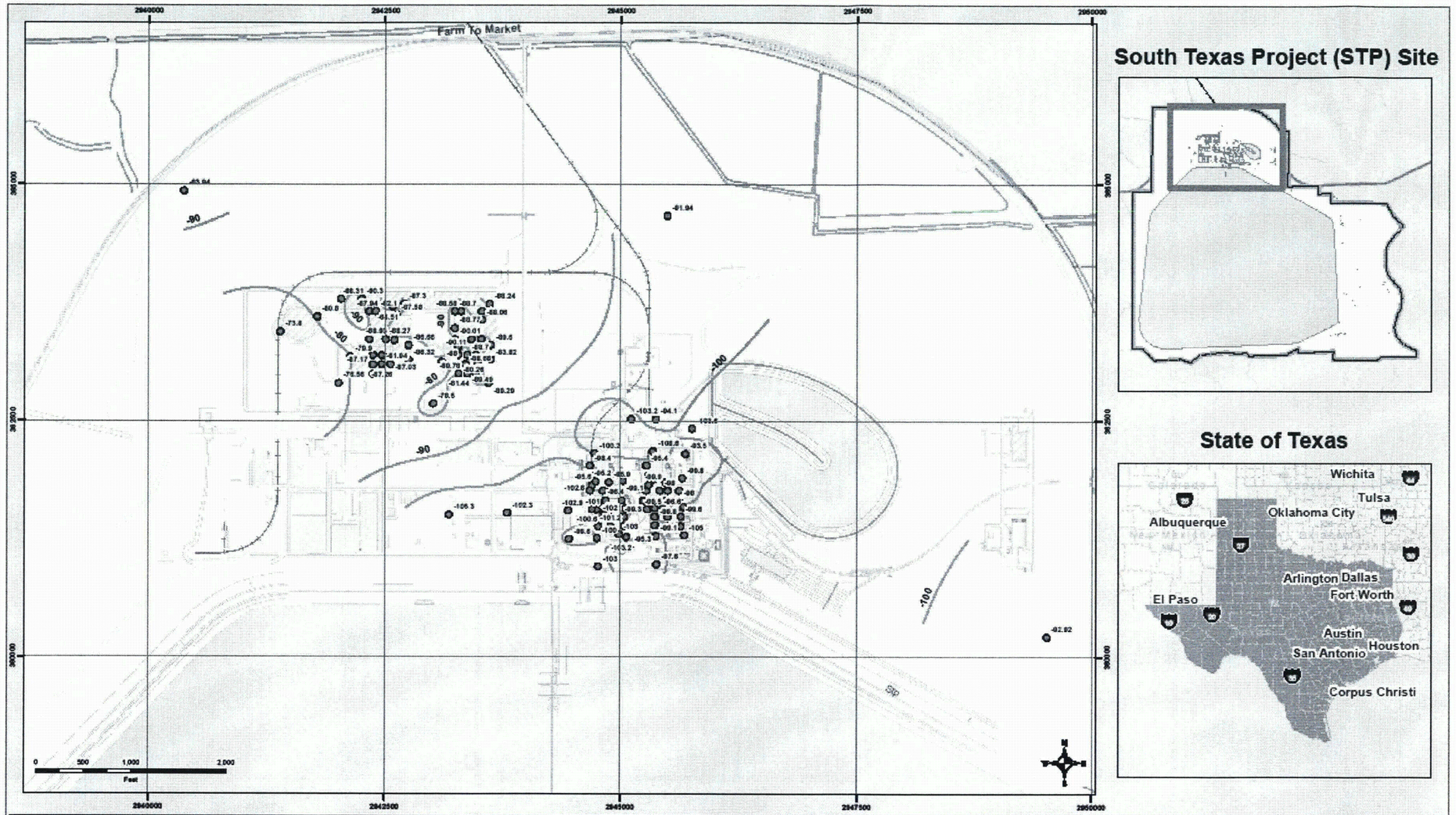
Farm To Market
2940000
2942500
2945000
2947500
2950000
392500
390000
387500
South Texas Project (STP) Site
State of Texas
Wichita
Tulsa
Oklahoma City
Albuquerque
Arlington
Dallas
Fort Worth
El Paso
Austin
Houston
San Antonio
Corpus Christi
0
500
1,000
2,000
Feet
Legend
Road Edge of Pavement
Railroad Centerline
Fence
Levee Centerline
Wall
Planned Structure
Existing Structure
Cooling Basin
STP Site Boundary
Bottom of Stratum H
Projection: Texas South Central State Plane, FIPS 4204
H. Datum: North American Datum 1927
V. Datum: National Geodetic Vertical Datum 1929
Display: Texas South Central State Plane
GIS Map Code:US-STPR-000062-R000D

RAI 02.04.12-17:

QUESTION:

In FSAR Section 2.4S.12.3.1, "Exposure Point and Pathway Evaluation", the applicant provides the first discussion and lays the foundation for alternate pathways considered in FSAR Section 2.4S.13. In FSAR Section 2.4S.13.1.2, "Conceptual Model", the applicant states "the downward hydraulic gradient between the Upper and Lower Shallow Aquifer indicates that there is no mechanism to lift the liquid effluent up into the Upper Shallow Aquifer." In this foundational section on pathways, please describe the process followed to consider and eliminate alternate conceptual models and determine the plausible alternative pathways. When doing so, describe and consider the effect the released liquid could have on the natural system, including thermal buoyancy effects and chelating agents. This is related to RAI 02.04.12-1.

RESPONSE:

Consideration, acceptance, and rejection of plausible groundwater flow alternative pathways is discussed in FSAR 2.4S.12.3.1, FSAR 2.4S.12.3.2, and FSAR 2.4S.13.1.2. The response to RAI 02.04.12-1 (hydrogeologic conceptual model development) provides a detailed description of the process followed to develop the site conceptual model of STP Units 3 & 4. Please refer to the above FSAR subsections and the response to RAI 02.04.12-1 for information related to development of conceptual models, and other plausible alternative pathways. The effects of thermal buoyancy and chelating agents identified in this RAI as potential mechanisms for alternative pathways are discussed in this response.

FSAR Section 2.4S.12.3.1 identifies the Shallow Aquifer as the most likely hydrogeologic unit to be impacted by an accidental liquid effluent release. The postulated accidental effluent release described in FSAR 2.4S.13.1.2 involves a release of 29,587 gallons of low conductivity waste (LCW) water from a LCW tank located at the lowest elevation of the Unit 3 Radwaste Building. The floor of the bottom elevation of the Radwaste Building is about 45 feet below grade, which is about five feet above the bottom of the Upper Shallow Aquifer. Therefore, if a release of heated liquid radwaste from this building occurred, the adjacent fill and Shallow Aquifer would likely be impacted.

The excavation for the foundation of the Unit 3 Reactor Building will extend about 90 feet below grade and into the Lower Shallow Aquifer. Backfill around this foundation and beneath adjacent buildings within the power block whose foundations are not as deep (e.g., the Radwaste Building) would likely create a conduit for vertical movement compared to the native aquifer material. As discussed in FSAR Section 2.4S.12.1.3, the Lower Shallow Aquifer consists of inter-bedded sand layers between depths of approximately 50 ft to 150 feet below ground surface. Therefore, the fill will span the Upper zone and an estimated 40 feet of the Lower zone of the Shallow Aquifer, effectively connecting the two zones hydraulically. Water level data collected from observation well pairs completed in the Upper and Lower Shallow Aquifers at Units 3 & 4 (OW-300 and -400 well series) are summarized in FSAR Table 2.4S.12-8. These data indicate that a consistent downward vertical hydraulic gradient ranging from about 0.106 to

0.225 exists between the two zones. This hydraulic gradient would provide the potential for some groundwater (and contaminants) from the Upper Shallow Aquifer to move downward into the Lower Shallow Aquifer, especially through the fill. However, the possibility of buoyancy effects that may result from a release of heated radwaste to overcome the natural downward hydraulic gradient is evaluated in this response as providing a plausible alternate pathway.

In a scenario involving potential buoyancy effects, the observed hydraulic conditions of the Shallow Aquifer, the fill, and the postulated LCW release described in FSAR 2.4S.13.1.2 were considered. FSAR Section 12.4S.12.1.4 indicates the potentiometric surface in the Upper Shallow Aquifer is 5 to 10 feet below grade in the area of Unit 3. Data from wells OW 308U and OW 332U summarized in FSAR Table 2.4S.12-16 indicate groundwater in this area has an average temperature ($Temp_{gw}$) of about 23.2° C (73.8° F). As postulated in FSAR Section 2.4S.13.1.2, liquids released from the LCW tank would collect at the bottom of the Radwaste Building, at a depth around 45 feet below grade. These liquids could be at a temperature ($Temp_{rw}$) as high as 80° C (176° F). In the unlikely event that a pathway through the walls or basement floor of the Radwaste Building developed, the higher hydraulic head within the Shallow Aquifer would cause groundwater to flow into the building until the potentiometric level inside and outside was equal. Consequently, the Radwaste liquid would mix with groundwater entering the structure.

To evaluate this scenario, the dimensions of the Radwaste Building where the mixing would occur were considered. The plan-view dimensions of the STP Unit 3 Radwaste Building are 214 feet by 124 feet, and the depth of this building below the water table is estimated to be about 35 feet assuming a depth to water table of 10 feet. Consequently, the estimated total volume of the Radwaste Building below the water table is:

$$(214\ ft)(124\ ft)(35\ ft) = 928{,}760\ ft^3$$ or roughly 6,950,000 gallons.

It is assumed that about half of this volume is void space (i.e., unoccupied by building and/or equipment infrastructure). So, the volume of void space in the Radwaste Building below the water table, where the mixing could occur, is estimated to contain about:

$$Volume_{mix} = (0.5)\ (6{,}950{,}000\ gal) = 3{,}475{,}000\ gallons.$$

There are four LCW tanks, each about 37,500 gallons in volume. Although only one tank ruptures in the postulated accident and it is unlikely that all four LCW tanks would be full simultaneously, to provide a conservative analysis of the potential heat transfer all four tanks are assumed to be filled with radwaste at the maximum design temperature of 80° C. Therefore, the heat in about 150,000 gallons of liquid radwaste would mix with the heat in the groundwater that floods the radwaste building.

The estimated volume of liquid radwaste ($Volume_{rw}$) providing heat is assumed to be the total volume of the four radwaste tanks or about 150,000 gallons, and the volume of ambient groundwater ($Volume_{gw}$) that can mix with the heated liquid radwaste is simply the difference between $Volume_{mix}$ and $Volume_{rw}$, or 3,325,000 gallons.

To estimate the resulting temperature of the mixing waters, a weighted average based on the equation for heat transfer ($Q = mc\Delta T$) and the First Law of Thermodynamics, is calculated using estimated quantities and temperatures of these waters. The temperature of water in the Radwaste Building after failure of the LCW Tank and flooding of the building with groundwater would be:

$$(Temp_{mix}) = [(Temp_{rw})(Volume_{rw}) + (Temp_{gw})(Volume_{gw})]/(Volume_{mix})$$
$$(Temp_{mix}) = (80^\circ C)(150{,}000 \text{ gal}) + (23.2^\circ C)(3{,}325{,}000 \text{ gal})/3{,}475{,}000 \text{ gal} = 25.7^\circ C$$

The difference in temperature between the mixture of spilled radwaste and groundwater in the Radwaste Building and ambient groundwater is estimated at about: $25.7^\circ C - 23.2^\circ C = 2.5^\circ C$.

Based on this analysis, the potential heat transfer from a release of radwaste water does not appear to be great enough to cause buoyancy. Consequently, this scenario is rejected as a likely alternate pathway.

A plausible alternate pathway involving chelating agents was also considered. Chelating agents, which can occur naturally in groundwater systems in the form of organic acids, or can result from a release of decontamination reagents, can influence the migration of radionuclides.

Decontamination reagents are used to remove activated metals and other radioactive components primarily associated with corrosion products that are deposited as films in the reactor coolant systems (RCS) of operating nuclear power plants. These films are periodically removed to reduce occupational radiation exposure and improve the thermal and hydraulic performance of the cooling system.

The three principal chemical decontamination processes that are currently used to reduce the films include the LOMI process, the CAN-DEREM process and the CITROX process (Reference 2). All of these decontamination processes use one or more chelating agents to dissolve the oxide coatings and to complex the released radionuclides that are loosened or broken up by strong oxidizing agents. The principal organic chelating agents in the decontamination solutions are: citric acid-EDTA in the CAN-DEREM process, formic acid-picolinic acid in the LOMI process, and citric acid-oxalic acid in the CITROX process (Reference 2).

The complexed radionuclides and any excess uncomplexed chelates are removed from the RCS onto cation-, anion-, and mixed-bed ion-exchange resins. These spent resins constitute the principal waste from the chemical decontamination process. The chelating agents would be chemically bound to the resins. Therefore, very little of the chelates would be available to react with liquid radwaste from the LCW tank during the postulated accident.

Because the ABWR design of STP Units 3 & 4 includes use of low-cobalt steel and injection of zinc into the RCS, it is very unlikely that chemical decontamination of the RCS will be required. Except during the decontamination process, the normal flow of radwaste to the LCW tank and through the ion-exchange resins does not contain chelating agents. If decontamination is required, the process would be completed with either the permanently- installed reactor water

cleanup (RWCU) system, or with a mobile skid-mounted treatment system. The resulting spent resins would be managed in the Unit 3 Radwaste Building in the spent resin tank (if the RWCU system is used) or in a high integrity container (HIC) (if a skid-mounted system is used) prior to off-site disposal. This waste would be the primary source of chelating agents that might influence the transport of radionuclides released to groundwater during the postulated accident.

Based upon the few studies of decontamination wastes identified in the literature, it appears that organic chelating agents can increase radionuclide leach rates by factors of 10 to 100 (Reference 2). However, available research on the adsorption of EDTA, oxalate and citrate and their metal complexes to soils and specific soil components, such as hydrous oxides, indicates that adsorption can be highly pH-dependent (Reference 2). Flow-through column tests show that the type of soil and pore water pH are important variables that combine with chelating agent concentration to affect radionuclide adsorption. All of the chelates can undergo what is termed "ligand-like" adsorption (i.e., adsorption of the chelates is strongest at low pH, decreases rapidly in the neutral pH region, and can be negligible at high pH [>8]). Data summarized in FSAR Table 2.4S.12-16 indicate the pH of groundwater in the Shallow Aquifer in the area of Units 3 & 4 is virtually neutral and ranges between 6.82 and 7.28.

Because of the more stable nature of complexes of EDTA with divalent transition metals (such as iron, cobalt and nickel) at higher pH values, EDTA can reduce adsorption of these metals onto soils or soil components. However, there is very good evidence for the adsorption of EDTA-metal complexes onto soil components, particularly on iron and aluminum oxides (Reference 2) which are abundant in alluvial soils such as those at STP. This adsorption of metal-chelate complexes can retard, rather than enhance, the migration of radionuclides in soils and sediments. As these complexes migrate through the aquifer from their point of release, dilution, interaction with competing cations in the pore fluids and adsorption reactions will result in dissociation of all but the strongest complexes. These factors make it especially difficult to predict the effects of EDTA on radionuclide transport in soils or sediments, and it appears that the enhanced migration of radionuclides via complexation with chelating agents may be limited to unique conditions (Reference 2).

Conditions that promote enhanced migration over long distances in an aquifer include high concentrations of organic chelating agents, low concentrations of competing cations, alkaline pH values, chelating agents with slow biodegradation rates, and kinetically inert complexes (Reference 2). The first of these conditions could be available in spent resin stored in the Unit 3 Radwaste Building prior to off-site disposal. However, should a rupture of the spent resin storage tank occur during the postulated accident involving a spill of LCW water, the chelating agents would be chemically bound to the resin and not readily available for reaction with radwaste. Any chelating agents that were released would be substantially diluted by flooding of the building that would occur if a pathway to the adjacent aquifer were completed.

Regarding the second condition, the Shallow Aquifer at the site is within the upper part of the Beaumont Formation, consisting of inter-layered sand, silt and clay. The clays and silts of the Shallow Aquifer can be expected to provide an abundant source of competing cation exchange minerals.

Regarding the third condition, alkaline pH conditions do not exist in the Shallow Aquifer, as noted above. The existence of the remaining two listed conditions is undetermined, but their effect likely would not outweigh the lack of high concentrations of chelating agents, abundance of cation exchange minerals and neutral pH in the Shallow Aquifer. For these reasons, it appears unlikely that the process of complexation of radionuclides with organic chelating agents would significantly affect the long-distance transport of radionuclides in the STP groundwater system.

Reference 1: NUREG/CR-6758, Radionuclide-Chelating Agent Complexes in Low-Level Radioactive Decontamination Waste; Stability, Adsorbtion and Transport Potential.

The end of Section 2.4S.13.1.2 of the FSAR will be revised as follows:

Other pathways that were considered and then rejected include (1) flow through the Upper Shallow Aquifer, (2) flow to the relief wells surrounding the MCR dike, (3) flow in the Deep Aquifer, ~~and~~ (4) the southwestward groundwater flow component on the western side of the STP site, (5) flow due to thermal buoyancy effects at the release, and (6) enhanced transport due to chelating agents.

(1) A release of liquid effluent from a ruptured LCW collector tank would flow to the lowest point in the Radwaste Building. The lowest point in the Radwaste Building (basement) is at the bottom of the Upper Shallow Aquifer. This consideration coupled with the presence of structural fill beneath the building from the Reactor Building excavation and the downward vertical hydraulic gradient between the Upper and Lower Shallow Aquifer indicates that ~~there is no mechanism to lift~~ migration of the liquid effluent up into the Upper Shallow Aquifer would be unlikely.

(2) Groundwater potentiometric surface maps (Figures 2.4S.12-17, 2.4S.12-19, and 2.4S.12-21) indicate that Shallow Aquifer groundwater flow is from, rather than toward, the MCR, thus precluding a transport pathway to the MCR.

(3) As discussed above, the Deep Aquifer is separated from the Shallow Aquifer by greater than 100 ft of low hydraulic conductivity silt and clay, and groundwater flow in the Deep aquifer within the site boundary appears to be controlled by pumping from onsite groundwater production wells. These factors suggest that it is unlikely that the Deep Aquifer would be a pathway for offsite release.

(4) The westward flow component in the Shallow Aquifer may represent a pathway from the Unit 4 Radwaste Building, however the site potentiometric maps (Figure 2.4S.12-17) indicate that flow is southward along the west side of the MCR and then turns back toward the southeast, on the south side of the MCR. This results in a similar flow pattern as Pathway

2, but with a much longer flow path distance to reach the Colorado River. Little Robbins Slough is not considered to be a discharge point for the Shallow Aquifer based on the potentiometric surface maps. Therefore, considering radioactive decay and adsorption, Pathway 2 results in a more conservative estimate of concentration at the river.

(5) To evaluate potential buoyancy effects due to a release of heated radwaste water from the Radwaste Building, the plan view dimensions (214 feet by 124 feet) and the depth of this building below the water table (35 feet assuming a depth to water table of 10 feet) are considered. The estimated total volume of the Radwaste Building below the water table is:

$(214\ ft)(124\ ft)(35\ ft) = 928{,}760\ ft^3$ or roughly 6,950,000 gallons.

Assuming about half of this volume is void space (i.e., unoccupied by building and/or equipment infrastructure), the volume of void space in the Radwaste Building below the water table, where mixing of groundwater with radwaste could occur, is estimated to be about:

$Volume_{mix} = (0.5)\ (6{,}950{,}000\ gal) = 3{,}475{,}000$ gallons.

The estimated volume of liquid radwaste ($Volume_{rw}$) is assumed to be the total volume of four radwaste tanks, or about 150,000 gallons, and the volume of ambient groundwater ($Volume_{gw}$) that can mix with the heated liquid radwaste is simply the difference between $Volume_{mix}$ and $Volume_{rw}$, or 3,325,000 gallons.

To estimate the resulting temperature of the mixing waters, a weighted average based on the equation for heat transfer ($Q = mc\Delta T$) and the First Law of Thermodynamics, is calculated using estimated quantities and temperatures of these waters:

$(Temp_{mix}) = [(Temp_{rw})(Volume_{rw}) + (Temp_{gw})(Volume_{gw})]/(Volume_{mix})$
$(Temp_{mix}) = (80°\ C)(150{,}000\ gal) + (23.2°\ C)(3{,}325{,}000\ gal)/3{,}475{,}000\ gal = 25.7°\ C$

The difference in temperature between the mixture of spilled radwaste and groundwater in the Radwaste Building and ambient groundwater is estimated at about: 25.7° C – 23.2° C = 2.5° C, and would not likely cause buoyancy.

(6) The effect that chelating agents might have on the transport of radionuclides released during the postulated accident has also been considered and is concluded not to be significant. Conditions that promote enhanced migration over long distances in an aquifer include (a) high concentrations of organic chelating agents, (b) low concentrations of competing cations, (c)

alkaline pH values, (d) chelating agents with slow biodegradation rates, and (e) kinetically inert complexes (Reference 2.4S.12-XX).

In condition (a), a rupture of the spent resin storage tank or a high integrity container (HIC) filled with spent resin in the Unit 3 Radwaste Building would have to also occur during the postulated accident involving a spill of LCW water. The chelating agents would be substantially diluted by flooding of the building that would occur if a pathway to the adjacent aquifer were completed.

In condition (b), the clays and silts of the Shallow Aquifer can be expected to provide an abundant source of competing cation exchange minerals.

In condition (c), the water quality tests conducted on the Shallow Aquifer do not indicate that alkaline pH conditions are present. The existence of the remaining two listed conditions is undetermined, but their effect likely would not outweigh the lack of high concentrations of chelating agents, abundance of cation exchange minerals and neutral pH in the Shallow Aquifer. For these reasons, it appears unlikely that the process of complexation of radionuclides with organic chelating agents would significantly affect the long-distance transport of radionuclides in the STP groundwater system.

The following new reference will be added to FSAR Section 2.4S.13:

2.4S.13 References

2.4S.13-XX, "Radionuclide-Chelating Agent Complexes in Low-Level Radioactive Decontamination Waste; Stability, Adsorbtion and Transport Potential," NUREG/CR-6758, February 2002.

RAI 02.04.13-1:

QUESTION:

In FSAR Section 2.4S.13.1, Direct Release to Groundwater, the applicant states that this section provides a conservative analysis of accidental release and migration. The process followed to consider, eliminate, and accept plausible alternative pathways (and conceptual models) is not specified. For example, when during the process followed were non-isothermal or buoyancy effects considered in the analysis of contaminant migration? Was the potential for chelating agents (organic compounds that alter sorption) being present considered, when determining the geochemical mobility of normally adsorbed radionuclides? This RAI is related to RAI 02.04.12-1 which requests that the process followed to arrive at the plausible alternative pathways be described more fully.

RESPONSE:

Consideration, acceptance, and rejection of plausible groundwater flow alternative pathways is discussed in FSAR 2.4S.12.3.1, FSAR 2.4S.12.3.2, and FSAR 2.4S.13.1.2. In addition, this RAI is related to both RAI 02.04.12-1 (hydrogeologic conceptual model development) and RAI 02.04.12-17 (thermal buoyancy and chelating agents). Please refer to these subsections as well as the responses to these RAIs to address the concerns raised in this RAI.

No COLA revision is required as a result of this RAI response.

RAI 02.04.13-4:

QUESTION:

In FSAR Section 2.4S.13.1.2, Conceptual Model, the applicant closes with a four-point summary of the alternate pathways. This needs elaboration, for example, (a) Under item (1), were thermal phenomena and buoyancy of heated water considered when making the statement "... there is no mechanism to lift the liquid ..."? While data are not included, the waste waters may be at elevated temperature relative to the ambient groundwater setting, and buoyancy may be a factor to be considered. (b) Under item (2), it is not clear that the schematic diagram in FSAR Figure 2.4S.12-21 represents actual data. In which tables do the data appear? Please provide a realistic three dimensional analysis. Complete the potentiometric surfaces of the Upper Shallow Aquifer, i.e., show contours underlying the MCR. The potentiometric surfaces of the Lower Shallow Aquifer indicate groundwater flow toward and under the MCR rather than around it. Why would the Upper Shallow Aquifer not also present an under rather than around pathway? Explain the reasons why the pathways presented are the most plausible, by providing the basis for them. (c) Under item (4), the issue of under versus around appears again. In addition, was the concept of the paleochannel raised in FSAR Section 2.4S.12.2.4.1 incorporated into the rationale when discarding this pathway?

RESPONSE:

Each of the three issues identified above will be addressed individually:

a) Thermal buoyancy of heated water was not considered under item (1) when that statement was made in the FSAR. However, the response to RAI 02.04.12-17 evaluates a thermal phenomena and buoyancy scenario such as the one described in this RAI. The response to RAI 02.04.12-17 concludes that in such a scenario, the temperature of the resulting effluent may be only about 2°C to 3°C warmer than the ambient groundwater and as a result, buoyancy would not likely occur.

No COLA revision is required as a result of Issue a) of this response.

b) FSAR Figure 2.4S.12-21 will be revised using groundwater levels tabulated in FSAR Table 2.4S.12-7. Stratigraphic information shown in this figure is derived from geologic logs of test borings and observation wells drilled for the Units 3 & 4 subsurface investigation (Reference 1).

The MCR was formed by constructing an approximately 45-foot high embankment on top of the existing ground surface. The MCR is unlined, and the level of the water contained by the MCR is up to 20 feet above the original grade. Groundwater levels in piezometers completed in the Upper Shallow Aquifer at the perimeter of the MCR appear to be several feet higher than those farther outside the perimeter. This indicates the hydrostatic head within the MCR induces seepage through the pond bottom.

Table 2.4S.12-XX (attached) lists groundwater elevations on March 1, 2003 in sets of piezometers distributed around the perimeter of the MCR. Each set consists of three piezometers located on a line perpendicular to the MCR embankment. The "A" position on this line is offset 11 feet landward from the centerline of the embankment. The "B" and "C" positions on the line are offset about 98 and 260 feet landward from the centerline of the embankment, respectively.

As shown in Table 2.4S.12-XX, the water level in the "A" position in each set of piezometers is highest, and those in the "B" and "C" positions are progressively lower. These data indicate that the hydraulic gradient in the Upper Shallow Aquifer beneath the entire length of the MCR embankment decreases in the landward direction, inducing groundwater flow outward from the MCR. This condition causes groundwater in the Upper Shallow Aquifer flowing toward the MCR from areas up-gradient to the northwest to be diverted and flow around rather than under the MCR.

Figure 2.4S.12-XX (attached) is a contour map of water-level elevations listed in Table 2.4S.12-XX in piezometers in the Upper Shallow Aquifer at the "A" position in each set around the MCR embankment, and in other available piezometers throughout the site. This map shows the piezometric surface in the Upper Shallow Aquifer beneath and in the vicinity of the MCR, and indicates that groundwater flow is outward from the MCR along the entire length of the embankment.

Hydrographs showing water levels in selected sets of piezometers around the MCR embankment from January 1998 to July 2002 indicate a decreasing hydraulic gradient in the Upper Shallow Aquifer from piezometers located in "A" positions to those at "C" positions and a resulting groundwater flow direction outward from the MCR.

This condition is also evidenced by the fact that most of the approximately 770 relief wells completed in the Upper Shallow Aquifer are at the toe of the embankment around the MCR. These are "flowing" wells because the hydraulic head imposed by the water level in the MCR induces a landward hydraulic gradient perpendicular to the embankment and potentiometric levels in the relief wells that are higher than the nearby ground surface elevation. The factors described above provide evidence that groundwater in the Upper Shallow Aquifer flowing toward the MCR from areas up-gradient to the northwest is diverted and flows around rather than under the MCR.

As discussed in FSAR Section 2.4S.12.1.3, the Lower Shallow Aquifer consists of inter-bedded sand and clay layers between depths of approximately 50 ft to 150 feet below ground surface. The sands within this unit are confined to semi-confined and FSAR Section 2.4S.12.2.5 discusses how the hydraulic separation between the Lower Shallow Aquifer and the Upper Shallow Aquifer may be discontinuous in places. However, the overall hydraulic separation between the two aquifers and the functioning relief well/sand blanket system is believed to limit the effect the hydrostatic head within the MCR has on the piezometric surface or flow direction in the Lower Shallow Aquifer. Observation wells are being installed to better monitor the effects of the MCR on the Shallow Aquifer.

For item b), the second bullet in the last paragraph of Section 2.4S.13.1.2 will be revised as follows:

2. Groundwater potentiometric surface maps (Figures 2.4S.12-17, 2.4S.12-19, 2.4S.12-XX and 2.4S.12-21) indicate that Shallow Aquifer groundwater flow is from, rather than toward, the MCR, thus precluding a transport pathway to the MCR.

The following paragraphs will be inserted before the last paragraph of Section 2.4S.12.2.2:

Table 2.4S.12-XX includes groundwater elevations for March 1, 2003 from piezometers distributed in sets of three around the perimeter of the MCR on a line perpendicular to the MCR embankment. The "A" position on this line is offset 11 feet landward from the centerline of the embankment. The "B" and "C" positions on the line are offset 98 and 260 feet landward from the centerline of the embankment, respectively.

Data summarized in Table 2.4S.12-XX indicate the water level in the "A" position in each piezometer set is highest, and those in the "B" and "C" positions are progressively lower. These data indicate that the hydraulic gradient in the Upper Shallow Aquifer beneath the entire length of the MCR embankment decreases in the landward direction, suggesting groundwater flow is outward from the MCR. This appears to cause groundwater flowing from upgradient regions of the Upper Shallow Aquifer to be diverted and flow around rather than beneath the MCR.

Figure 2.4S.12-XX is a contour map of water-level elevations in piezometers in the Upper Shallow Aquifer at the "A" position in each set around the MCR embankment, and in other available piezometers throughout the site. This map shows the piezometric surface in the Upper Shallow Aquifer beneath and in the vicinity of the MCR, and indicates that groundwater flow is outward from the MCR along the entire length of the embankment.

As discussed in FSAR Section 2.4S.12.1.3, the Lower Shallow Aquifer consists of inter-bedded sand and clay layers between depths of approximately 50 ft to 150 feet below ground surface. The sands within this unit are confined to semi-confined and FSAR Section 2.4S.12.2.5 states that the hydraulic separation between the Lower Shallow Aquifer and the Upper Shallow Aquifer may be discontinuous in places. However, the overall hydraulic separation between the two aquifers and the functioning relief well/sand blanket system is believed to limit the effect the hydrostatic head within the MCR has on the piezometric surface or flow direction in the Lower Shallow Aquifer.

c) The concept of a paleochannel as mentioned in FSAR Section 2.4S.12.2.4.1 is discussed in the response to RAI 02.04.12-15. This response states that there are insufficient data to establish the existence of a preferential flow path within the Shallow Aquifer. Because the paleochannel is not a confirmed feature, it was not specifically included in the pathway

analysis. However, the sensitivity analysis presented in FSAR Section 2.4S.13 includes a pathway analysis where relatively shorter travel times and distances – such as that which would be expected to occur if a paleochannel existed – were considered.

No COLA revision is required as a result of Issue c) of this RAI response.

References:

1. "Geotechnical Subsurface Investigation Data Report, Combined Operating License Application (COLA) Project, South Texas Project (STP)," Report by MACTEC Engineering and Consulting, Inc., April 2007.

Table 2.4S.12-XX

Summary of Water Levels in the Upper Shallow Aquifer on March 1, 2003

SOUTH TEXAS PROJECT - ABWR Unit 3 & 4 COL Application
Matagorda County, Texas

Piezometers Around the Perimeter of the MCR				
Piezometer No.	Embankment Station	Bottom Elevation (ft, MSL)	Location on Embankment	Water-Level Elevation on 3/1/2003 (ft, MSL)
P5	7+00	-6.0	A	29.00[a]
P6	7+00	-6.0	B	-
P7	7+00	-6.0	C	21.40
P9	11+00	-1.0	A	27.90[a]
P10	11+00	-1.0	B	22.90[a]
P11	11+00	-1.0	C	22.10
P13	20+00	-15.0	A	26.30[a]
P14	20+00	-15.0	B	22.60
P15	20+00	-15.0	C	24.50
P17	40+20	-10.0	A	23.30[a]
P18	40+20	-10.0	B	21.70
P19	40+20	-10.0	C	20.80
P21	59+60	-9.0	A	24.10[a]
P22	59+60	-9.0	B	21.60
P23	59+60	-9.0	C	-
P25	79+80	-15.0	A	23.70[a]
P26	79+80	-15.0	B	22.60
P27	79+80	-15.0	C	21.00
P29	100+20	-5.0	A	32.70[a]
P30	100+20	-5.0	B	30.00
P34	130+40	-7.0	A	29.20[a]
P35	130+40	-7.0	B	24.70
P36	130+40	-7.0	C	-
P38	160+00	0.0	A	38.60[a]
P39	160+00	0.0	B	20.30
P40	160+00	0.0	C	16.40
P42	180+25	-1.0	A	-
P43	180+25	-1.0	B	24.20
P44	180+25	-1.0	C	13.10
P46	200+20	-7.0	A	24.50[a]
P47	200+20	-7.0	B	21.60
P48	200+20	-7.0	C	17.60
P50	219+80	-25.0	A	-
P51	219+80	-25.0	B	17.90
P52	219+80	-25.0	C	16.60

Piezometers Around the Perimeter of the MCR				
Piezometer No.	Embankment Station	Bottom Elevation (ft, MSL)	Location on Embankment	Water-Level Elevation on 3/1/2003 (ft, MSL)
P53	226+40	-20.0	A	16.40[a]
P54	226+40	-20.0	B	15.00
P55	226+40	-20.0	C	12.00
P57	240+00	-23.0	A	19.20[a]
P58	240+00	-23.0	B	17.40
P59	240+00	-23.0	C	14.90
P61	260+25	-13.0	A	17.40[a]
P62	260+25	-13.0	B	15.30
P63	260+25	-13.0	C	14.00
P64	283+00	-9.0	A	18.90[a]
P65	283+00	-9.0	B	14.40
P66	283+00	-9.0	C	13.10
P68	300+00	-19.0	A	19.30[a]
P69	300+00	-19.0	B	16.90
P70	300+00	-19.0	C	13.80
P72	320+00	-8.0	A	16.80[a]
P73	320+00	-8.0	B	14.40
P74	320+00	-8.0	C	12.40
P77	359+60	0.0	A	22.60[a]
P78	359+60	0.0	B	20.40
P79	359+60	0.0	C	15.20
P81	380+00	-24.0	A	21.60[a]
P82	380+00	-24.0	B	19.80
P83	380+00	-24.0	C	17.30
P85	400+50	-22.0	A	24.70[a]
P86	400+50	-22.0	B	23.30
P87	400+50	-22.0	C	16.80
P89	420+00	-22.0	A	20.30[a]
P90	420+00	-22.0	B	18.70
P91	420+00	-22.0	C	16.00
P93	440+20	-4.0	A	21.60[a]
P94	440+20	-4.0	B	19.20
P95	440+20	-4.0	C	16.20
P97	460+10	-22.0	A	-
P98	460+10	-22.0	B	19.20
P99	460+10	-22.0	C	16.40
P101	491+00	-22.0	A	26.50[a]
P102	491+00	-22.0	B	25.20
P103	491+00	-22.0	C	22.80
P105	511+00	-22.0	A	28.30[a]
P106	511+00	-22.0	B	28.10
P107	511+00	-22.0	C	23.80

Piezometers Around the Perimeter of the MCR				
Piezometer No.	Embankment Station	Bottom Elevation (ft, MSL)	Location on Embankment	Water-Level Elevation on 3/1/2003 (ft, MSL)
P109	531+00	-13.0	A	32.80[a]
P110	531+00	-13.0	B	30.40
P111	531+00	-13.0	C	27.50
P113	550+50	-3.0	A	27.70[a]
P114	550+50	-3.0	B	25.60
P115	550+50	-3.0	C	23.00
P116	570+35	-11.0	A	27.50[a]
P117	570+35	-11.0	B	25.59
P118	570+35	-11.0	C	23.90
P120	590+40	+4	A	35.50[a]
P121	590+40	+4	B	30.90
P122	590+40	+4	C	25.80
P124	610+00	-12.0	A	30.70[a]
P125	610+00	-12.0	B	28.50
P126	610+00	-6.0	C	26.80
P128	629+00	-13.0	A	32.30[a]
P129	629+00	-13.0	B	28.80
P130	629+00	-13.0	C	26.00
P132	652+20	-16.0	A	-
P133	652+00	-16.0	B	-
P134	652+00	-16.0	C	25.50
Site Piezometers				
225A-02	-	-	-	19.27[b]
274C	-	-20.7	-	19.98[b]
435	-	-31.2	-	19.97[b]
446A	-	-39.8	-	0.83[b]
447A	-	-38.6	-	8.05[b]
601	-	-14.1	-	23.36[b]
602A	-	-16.7	-	23.40[b]
603B	-	-12.3	-	24.49[b]
MCR	-	~+20	-	~47[a]

Notes:
"A" piezometer offset 11 feet landward from centerline of embankment.
"B" piezometer offset 98 feet landward from centerline of embankment.
"C" piezometer offset 260 feet landward from centerline of embankment.
[a] measurement on 3/10/2003
[b] measurement on 2/1/2003

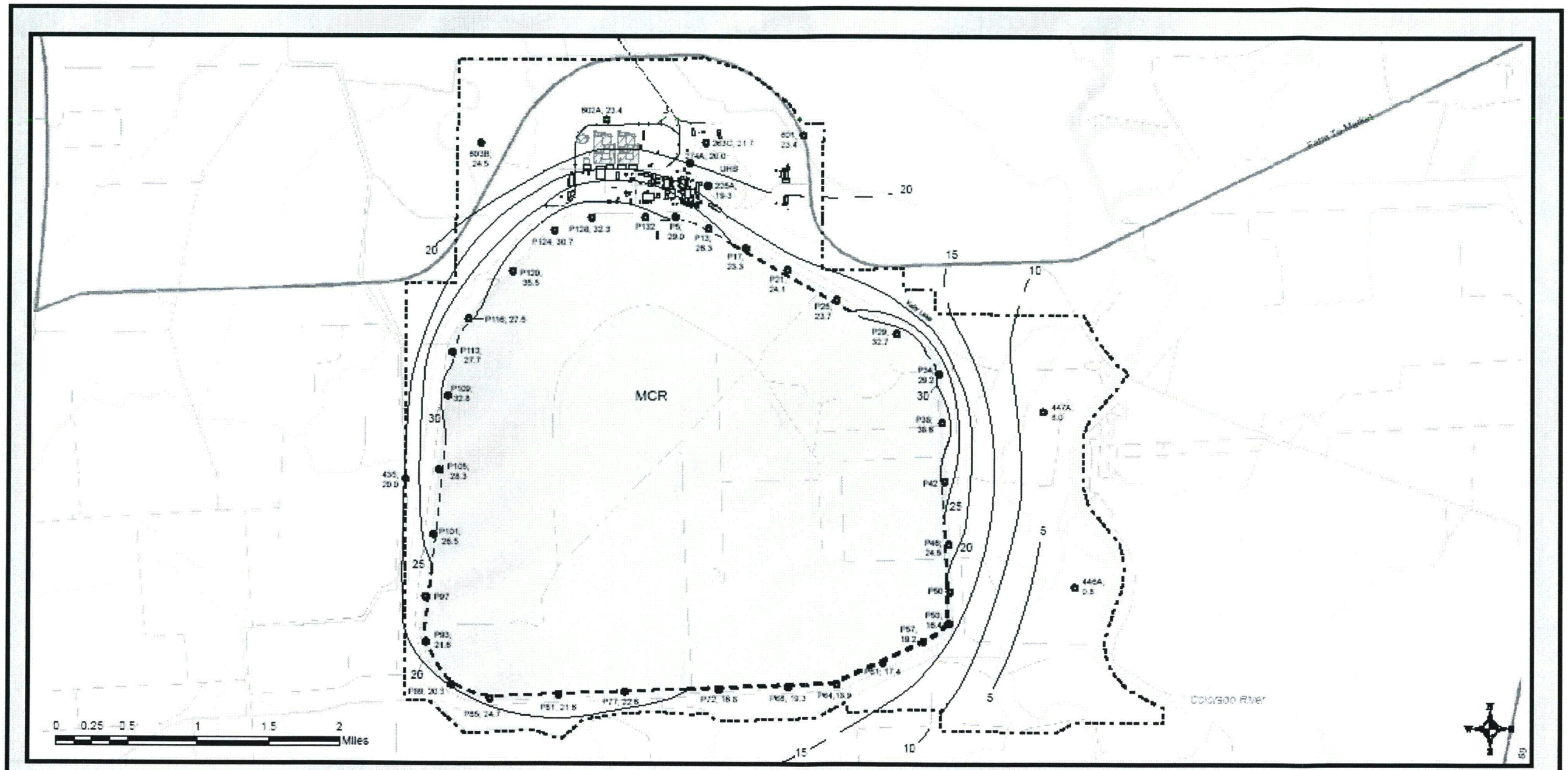

Figure 2.4S.12 - XX
Potentiometric Surface in the Upper Shallow Aquifer [1, 2, 3]

Projection: South Central Texas State Plane
Datum: North American Datum 1927

Notes:
1. Locations of pelzometers are approximate.
2. Water levels in MCR Embankment pelzometers on March 1, 2003. Water levels in site pelzometers on February 1, 2003.
3. Surface water elevation in MCR was approximately 47 feet MSL from January to April 2003.

RAI 02.04.13-8:

QUESTION:

While the applicant describes the importance of including chain decay progeny calculations in the dosimetric calculations, not all progeny results are presented. Describe and present the progeny results. Include for example, Mo-99 → Tc-99, Tc-99m → Tc-99, and Te-129m → I-129.

RESPONSE:

FSAR Figure 2.4S.13-1 shows the decay chains (including the three requested decay chains) that were considered when analyzing the transport of radionuclides for the postulated release described in FSAR Section 2.4S.13. FSAR Table 2.4S.13-2 provides calculations for each of these decay chains. In accordance with Reference 2.4S.13-1, the decay chains were truncated at the member progeny where the incremental dose from the total energy from all radiation emitted over a 100-year period is not significant.

No COLA revision is required as a result of this RAI response.

RAI 02.04.13-9:

QUESTION:

Reconcile the following statements in the FSAR Section 2.4S.13.2: (a) "Because there are no outdoor tanks in the LWMS that could release radioactive effluent, no accident scenario could result in the release of effluent directly to the surface water" and (b) "A flood, such as that caused by an MCR dike breach, could flood the Radwaste Building and potentially release radioactive materials into the environment. A flood of this magnitude would disperse and dilute the radionuclide concentration of a surface water spill."

RESPONSE:

To reconcile both statements, the first paragraph of FSAR Section 2.4S.13.2 will be revised as follows:

> The design of the Liquid Radioactive Waste System (LWMS) for STP 3 & 4 as described in Section 11.2 specifies that all liquid radwaste tanks are to be contained inside of the Radwaste Building. ~~indoors and the~~ The Radwaste Building will have Seismic Category I walls and basemat of sufficient dimensions to contain all liquid radwaste. ~~Because t~~ There are no outdoor tanks in the LWMS that could release radioactive effluent~~, no~~. Therefore, the most plausible accident scenario that could result in the release of effluent directly to ~~the~~ surface water is a rapid and catastrophic flood, such as that caused by a breach of the MCR embankment, inundating the Radwaste Building coinciding with leakage from the indoor tanks on the basement level of the Radwaste Building.

RAI 02.05.01-12:

QUESTION:

In Section 2.5S.1.2.4.3, you concluded that "there was no observed surface expression of this growth fault to suggest that it has been active since the deposition of the late Pleistocene Beaumont Formation." This conclusion depends on an estimate of the age of the geomorphic surface in the site area and of the rate of erosion of a scarp. How old is the surface in the site area? Please describe over what period of time, fault scarps of various heights can be preserved (such as 0.5 m and 1.0 m).

RESPONSE:

There are two issues identified within this RAI question, which can be summarized as:

1. How old is the surface in the site area?

2. Please describe over what period of time, fault scarps of various heights can be preserved (such as 0.5 m and 1.0 m).

Each of these issues will be addressed individually.

Issue 1

The geomorphic surface within the STP 3 & 4 site area is the informal Bay City valley fill subdivision of the Beaumont Formation (Reference 1) (Figure 2.5S.1-14). The Bay City valley fill is a highly heterogeneous fluvial-deltaic deposit that is composed of sands, silts, clays and estuarine muds (Reference 1). Based on thermoluminescence dating, Blum and Aslan (Reference 1) estimate that the Bay City fill was deposited between approximately 100,000 to 150,000 years ago.

No COLA revision is required as a result of Issue 1 of this RAI response.

Issue 2

As discussed in Subsection 2.5S.1.2.4.2, surface deformation associated with Quaternary-active growth faults in the greater site area is characterized by broad monoclinal folding and flexure extending on the order of several kilometers along the strike of the growth faults (Reference 2). Within the greater site area, this type of monoclinal folding warps the Beaumont Formation surface and has produced a gentle but distinct change in surface gradient where folding has steepened the Beaumont surface. This geomorphic expression should not be described as a scarp because there is no discrete break or offset in the land surface.

The question in issue 2 is essentially how long can the observable change in surface gradient across these low-relief monoclinal folds be preserved. The topographic profiles across growth faults discussed in Subsection 2.5S.1.2.4.2 show slopes for the steepened limb of the monoclinal fold of approximately 0.3° to 0.7° (equivalent to several feet of warping in the Beaumont Formation occurring over hundreds of horizontal feet), in contrast to the approximately 0.03° regional slope of the Beaumont Formation (Reference 3). The amplitude of the folding shown in Figure 2.5S.1-46 is extremely low despite the pronounced appearance of the folding in the Beaumont surface because of the over 100 times vertical exaggeration used in the figure.

Due to a lack of detailed information on erosion rates and erodability of materials within the site area (e.g., Reference 4), it is not possible to confidently state the maximum or total time monoclinal folding from growth faulting will persist as a geomorphic feature on the landscape. However, available observations within the greater site vicinity and throughout the coastal plain provide some broad constraints on the minimum amount of time low-relief geomorphic features persist within the greater site area. These observations are described below, and they lead to the conclusion that monoclinal folds in the Beaumont Formation, like those associated with fault GMO, are capable of persisting as modest, local increases in surface slope for tens of thousands to hundreds of thousands of years. The implication of this conclusion is that a geomorphic surface free of monoclinal folding within the site area can be precluded from having experienced any surface deformation related to growth faulting at least since the deposition of the surface (i.e., approximately 100,000 years for the youngest unit of the Beaumont Formation (Reference 1)).

The monoclinal flexures associated with growth faults could be removed by either: (1) deposition and erosion associated with active fluvial systems, or (2) paired erosion and deposition from small-scale, non-fluvial processes that remove sediments from the upper limb of the monoclinal fold and deposit them on the lower limb, essentially diffusing the distinct change in surface gradient and reducing the surface gradient of the steepened surface. For either of these processes to remove evidence of a growth fault, they need to occur over the entire along-strike extent of the monoclinal fold, commonly several miles or more (Reference 2).

Large-scale fluvial deposition and erosion within a river valley could mask a growth fault monoclinal fold and may be able to mask the entire lateral extent of the fold if the river system migrated extensively (e.g., see the extent of the Bay City valley fill near the STP 3 & 4 site in Figure 2.5S.1-14). The occurrence of either of these activities would be marked by the deposition of sediments younger than the age of the folding; any subsequent activity on the growth fault would form a new monoclinal fold. Therefore, the absence of a scarp within a region of Late Pleistocene and younger sediments precludes growth fault activity from having occurred within that region since deposition of the sediments. An inherent assumption of this conclusion is that non-fluvial processes are not capable of removing the monoclinal fold. This assumption is supported, as described below.

Small-scale, non-fluvial surface processes (e.g., sheet, rill, gulley, and wind erosion as well as associated deposition) are also not likely to mask monoclinal folds from growth fault. These processes are generally thought to be a function of slope and curvature with rates increasing with

both greater slope and curvature (Reference 5). The average slope of Pleistocene deposits (approximately 0.03°) (Reference 3) and the increased slope of the growth fault GMO fold (0.3° to 0.7°; see Subsection 2.5S.1.2.4.2.2.2) within the site area are both very small (i.e., essentially zero), providing little to no topographic gradient or gravitational force to drive these processes (Reference 5). The observed change in slope between the monoclinal folds associated with growth fault GMO and the Beaumont Formation is also very small and occurs over considerable distances (Figure 2.5.S1-46), again indicating that there is very little forcing to drive these erosive processes. Therefore, the primary geomorphic process acting in these regions is most likely pedogenesis (i.e., soil development), which is not capable of removing monoclinal folds of the scale observed with growth fault GMO.

The primary evidence supporting the conclusion that non-fluvial surface processes in the site area are not capable of removing monoclinal folds similar to that observed with growth fault GMO is the presence of well-developed and mature soils that have likely had thousands to tens of thousands of years to develop. The presence of these soils suggests that there has not been any significant erosion or deposition of the Beaumont Formation surface since development of the soils began. The primary soils near the projection of growth fault GMP include the Bacliff, Edna, Dacosta, and Laewest series formed in the Pleistocene Beaumont Formation (Reference 4). The Bacliff, Edna, and Dacosta soils (vertisol, alfisol, and mollisol, respectively) are the more extensive soils, and the Laewest series (vertisol) is less extensive.

Vertisols in the Texas Coastal Plain (e.g., the Bacliff and Laewest series) are generally Late Pleistocene in age and are estimated to be no older than 35,000 to 40,000 years old (Reference 6). The Bacliff series soil lacks Bt (clay accumulation) and Bk (carbonate accumulation) horizons, but the C horizon is strong brown to reddish yellow (7.5YR5/6, 7.5YR6/6, Munsell soil notation) suggesting a moderate amount of time to accumulate iron-based precipitates. The Laewest series also lacks a Bt horizon but has two Bkss horizons (Reference 4). Bk horizons, or calcic horizons, also require substantial time for accumulation of carbonate in the soil profile (Reference 7).

Within the Dacosta and Enda series, up to five Bt soil horizons are identified, and range in total thickness from 84 to 54 inches, respectively. Bt horizons indicate production and translocation (downward movement and accumulation) of clay, resulting in the well-developed and argillic (i.e., clay-rich) pedogenic horizons. Development of thick Bt horizons generally is a function of time. The presence of numerous Bt horizons, collectively over four-feet-thick, suggests a prolonged period of landscape stability and soil development for these series of greater than thousands of years, and possibly greater than tens of thousands of years (Reference 7). In comparison with the Bacliff and Laewest series, the presence of the Bt horizons within the Dacosta and Edna soils suggests these soils may have developed over a longer time period than the Bacliff and Laewest soils. Combined, the different soils of the site area all support the conclusion that erosion and deposition within the site area has been minimal over a period of tens of thousands to hundreds of thousands of years, thus lending confidence to the interpretation that the absence of observed monoclinal folding is positive evidence for no growth fault activity since the deposition of sediments that are subaerially exposed within the site area (i.e., the Beaumont Formation).

No COLA revision is required as a result of Issue 2 of this RAI response.

References:

1. Blum, M.D., and Aslan, A., 2006, Signatures of climate vs. sea-level change within incised valley-fill successions: Quaternary examples from the Texas Gulf Coast: Sedimentary Geology, v. 190, p. 177-211.
2. Verbeek, E., R., 1979, Surface faults in the Gulf coastal plain between Victoria and Beaumont, Texas.: Tectonophysics, v. 52, p. 373-375.
3. Winker, C.D., 1979, Late Pleistocene Fluvial-Deltaic Deposition: Texas Coastal Plain and Shelf [MA thesis]: Austin, TX, University of Texas at Austin.
4. Hyde, H.W., 2001, Soil survey of Matagorda County, Texas, United States Department of Agriculture, Natural Resources Conservation Service, in cooperation with Texas Agricultural Experiment Station, p. 171.
5. Easterbrook, D.J., 1993, Surface Processes and Landforms: New York, NY.
6. Driese, S.G., Nordt, L.C., Lynn, W.C., Stiles, C.A., Mora, C.I., and Wilding, L.P., 2005, Distinguishing Climate in the Soil Record Using Chemical Trends in a Vertisol Climosequence from the Texas Coast Prairie, and Application to Interpreting Paleozoic Paleosols in the Appalachian Basin, U.S.A. : Journal of Sedimentary Research, v. 75, p. 339-349.
7. Birkeland, P.W., 1999, Soils and Geomorphology, third edition: New York, Oxford University Press.

RAI 02.05.01-13:

QUESTION:

If comparison of growth faults identified or precluded in the UFSAR for STP 1 and 2 with the new data described in this report is "problematic," as stated in Section 2.5S.1.2.4.3, please explain why growth faults GMH and GMK could not project through the STP COLA site and why growth faults GMO and GMI could not project through the reservoir.

RESPONSE:

In the summary of Subsection 2.5S.1.2.4.3, the statement about correlating growth faults from the Geomap data (Reference 1) to growth faults identified in the UFSAR for STP Units 1 and 2 (Reference 2) should refer to growth faults GML and GMK, not faults GMI and GMK. In Figures 2.5S.1-45 and 2.5S.1-43 the fault on the west side of the site area previously labeled GMI should be labeled GML.

For growth faults GMH, GMI, GMK and GML the constraints on the positions of the faults from the Geomap data (Geomap, 2007) can be summarized as follows:

- As shown in Figure 2.5S.1-43, the surface projection of growth fault GMK extends to within approximately 3 miles of the site. This extent is based on the A and B horizon Geomap data (Reference 1) that identify the fault at depths of approximately 7500 feet and 8500 feet, respectively, and were used to estimate the surface projection of the growth fault (see Subsection 2.5S.12.4.2.2.1). In these horizons growth fault GMK only extends to within approximately 3 miles of the cooling reservoir;

- As shown in Figure 2.5S.1-43, the surface projection of growth fault GML extends to within approximately 5 miles of the site. This extent is based on the A and B horizon Geomap data (Reference 1) that identify the fault at depths of approximately 7500 feet and 8500 feet, respectively, and were used to estimate the surface projection of the growth fault (see Subsection 2.5S.12.4.2.2.1). In these horizons growth fault GML only extends to within approximately 5 miles of the cooling reservoir;

- As shown in Figure 2.5S.1-42, the surface projection of growth fault GMI extends to within approximately 4 miles of the cooling reservoir. This extent is based on the A and B horizon Geomap data (Reference 1) that identify the fault at depths of approximately 9000 feet and 11,000 feet, respectively, and were used to estimate the surface projection of the growth fault (see Subsection 2.5S.12.4.2.2.1). In these horizons growth fault GMI only extends to within approximately 4 miles of the cooling reservoir; and

- As shown in Figure 2.5S.1-43, the surface projection of growth fault GMH extends to within approximately 4 miles of the site. This extent is based on the A and B horizon Geomap data (Reference 1) that identify the fault at depths of approximately 8500 feet and 11,000 feet, respectively, and were used to estimate the surface projection of the

growth fault (see Subsection 2.5S.12.4.2.2.1). In these horizons growth fault GMH only extends to within approximately 4 miles of the cooling reservoir.

It is possible that one or all of growth faults GML, GMK, GMI, and GMH extend beyond their position as defined by the Geomap data (Reference 1) (i.e., growth fault GMK and/or GML may extend further east and GMH and/or GMI may extend further west). The position of the faults in the Geomap data (Reference 1) is primarily based on interpretations of the faults from well logs, and these four faults terminate towards the site in a region where there is very little well data that could be used to constrain the faults. This coincidence between the lack of well data and the mapped termination of the faults suggests that the fault terminations may be due to a lack of well constraints and not the absence of the faults at depth.

The inability of the Geomap data (Reference 1) to potentially constrain the position of growth faults GMH, GMI, GMK and GML closer to the site and the cooling reservoir is not considered significant because of the multidisciplinary approach used to identify potential growth faults within the site vicinity and site area, in particular the extensive seismic reflection data collected as part of the UFSAR for STP Units 1 and 2 (Reference 2) (see STP Units 3 & 4 FSAR Subsection 2.5S.1.2.4.2). The Geomap growth faults (Reference 1) cannot be directly correlated with the faults identified within the UFSAR for STP Units 1 and 2 (Reference 2) because none of the seismic reflection lines from the UFSAR cross the Geomap (Reference 1) growth fault traces. However, given the number, location, and geometry of the shallow seismic lines identified in the UFSAR for STP Units 1 and 2 (Reference 2) (e.g., TXO and Jaecon lines; see STP Units 1 and 2 UFSAR Subsection 2.5.1.2.5.3) as well as the imaged subsurface relations documenting no deformation of Miocene and younger strata beneath the site or cooling reservoir, the conclusion of the UFSAR that there are no shallow growth faults beneath the site or cooling reservoir is reasonable. In addition, COLA Subsection 2.5S.1.2.4.2.2.2 describes detailed field investigations undertaken to identify any potential surface features related to growth fault activity, and no features were found that intersect the site or the cooling reservoir.

As discussed in Subsection 2.5S.1.2.4.2.2.2, unlike the faults discussed above, growth fault GMO can be directly correlated to a fault identified within the UFSAR for STP Units 1 and 2 (Reference 2): growth fault STP12I. Therefore, it is inferred that these two growth faults are the same fault. The projection of growth fault STP12I/GMO does pass through the cooling reservoir. However, as discussed in Subsection 2.5S.1.2.4.2.2.2 and the UFSAR for STP Units 1 and 2 (Reference 2), it was concluded that the post-Beaumont surface deformation associated with the growth fault does not trend eastward into the cooling reservoir.

References:

1. Geomap, 2007, Upper Texas Gulf Coast Mapping Service maps 327 and 328. Licensed from Geomap Company to William Lettis and Associates, Inc. from February 1, 2007 to January 31, 2008.
2. STPEGS, Rev 13, STPEGS Updated Final Safety Analysis Report, Units 1 and 2, Revision 13.

The third paragraph in FSAR section 2.5S.1.2.4.3 will be replaced with the following text:

The UFSAR for STP 1 & 2 (Reference 2.5S.1-7) also identified several approximately west-southwest-striking growth faults at the latitude of the STP 3 & 4 site footprint at depths ranging from 6000 ft. to 11,000 ft. (i.e., growth faults Matagorda STP12D, STP12E and STP12H). One or more of these structures likely correlates with growth faults Matagorda GML and GMK (Reference 2.5S.1-124), which strike into the site area from the west (Figure 2.5S.1-42 [References 2.5S.1-29, 2.5S.1-124, 2.5S.1-150, 2.5S.1-151, 2.5S.1-152, and 2.5S.1-153]) and are mapped to within approximately 5 miles or less of STP 3 & 4 (Figure 2.5S.1-43 [References 2.5S.1-7, 2.5S.1-124, and 2.5S.1-151]). The growth faults identified within the UFSAR for STP 1 & 2 (Reference 2.5S.1-7) cannot be directly correlated with growth fault GML or GMK because the seismic reflection lines from the UFSAR for STP 1 & 2 (Reference 2.5S.1-7) do not cross the Geomap fault traces for growth faults GML and GMK. However, the reflection lines from the UFSAR for STP 1 & 2 (Reference 2.5S.1-7) combined with the new studies presented here support the conclusion that there are no shallow growth faults that intersect either the site or the cooling reservoir.

Figures 2.5S.1-43 and 2.5S.1-45 will be replaced with the following revised figures on the next pages.

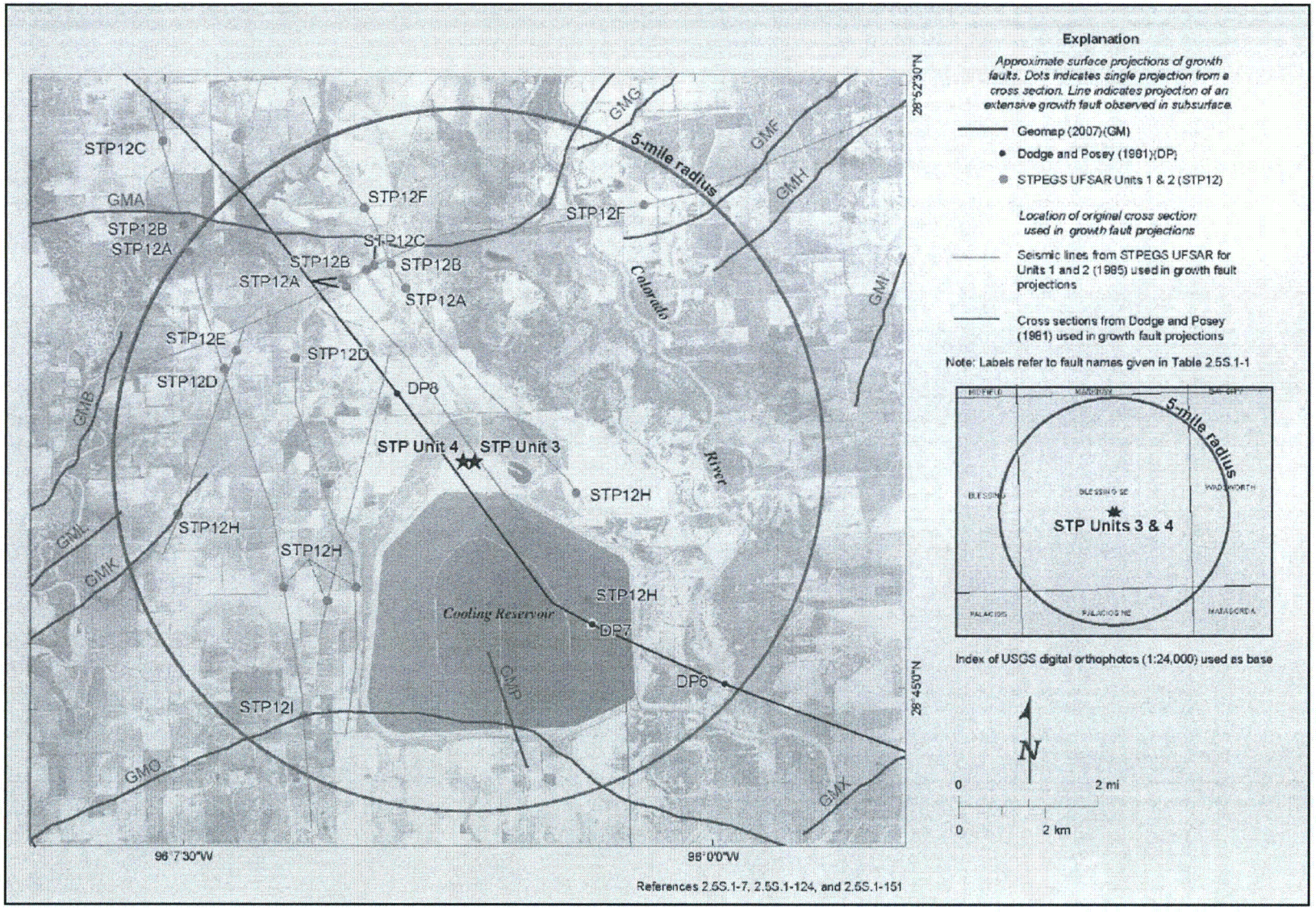

Figure 2.5S.1-43 Site Vicinity (5-mile radius) Growth Fault Surface Projections [Previous version]

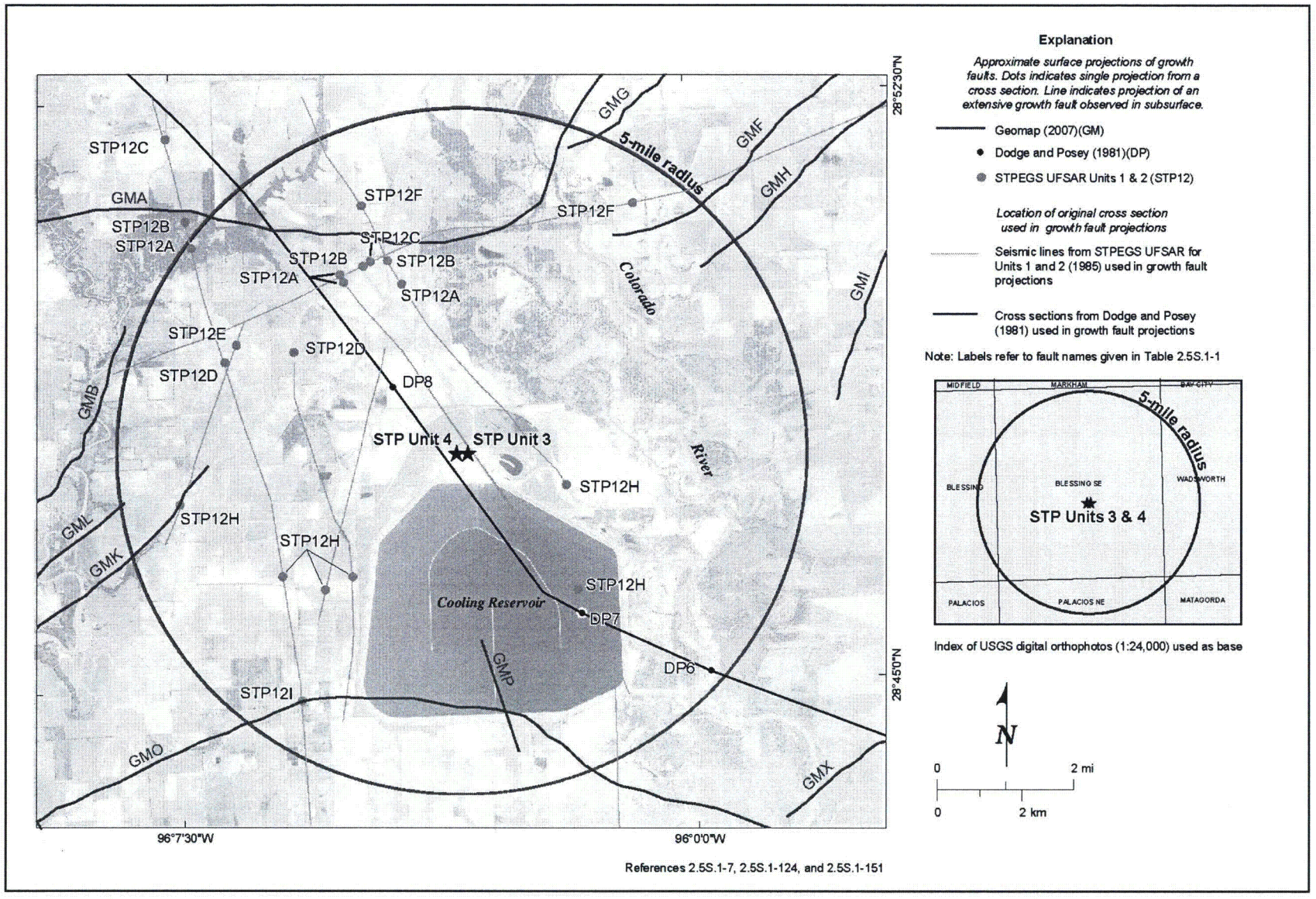

Figure 2.5S.1-43 Site Vicinity (5-mile radius) Growth Fault Surface Projections [New version]

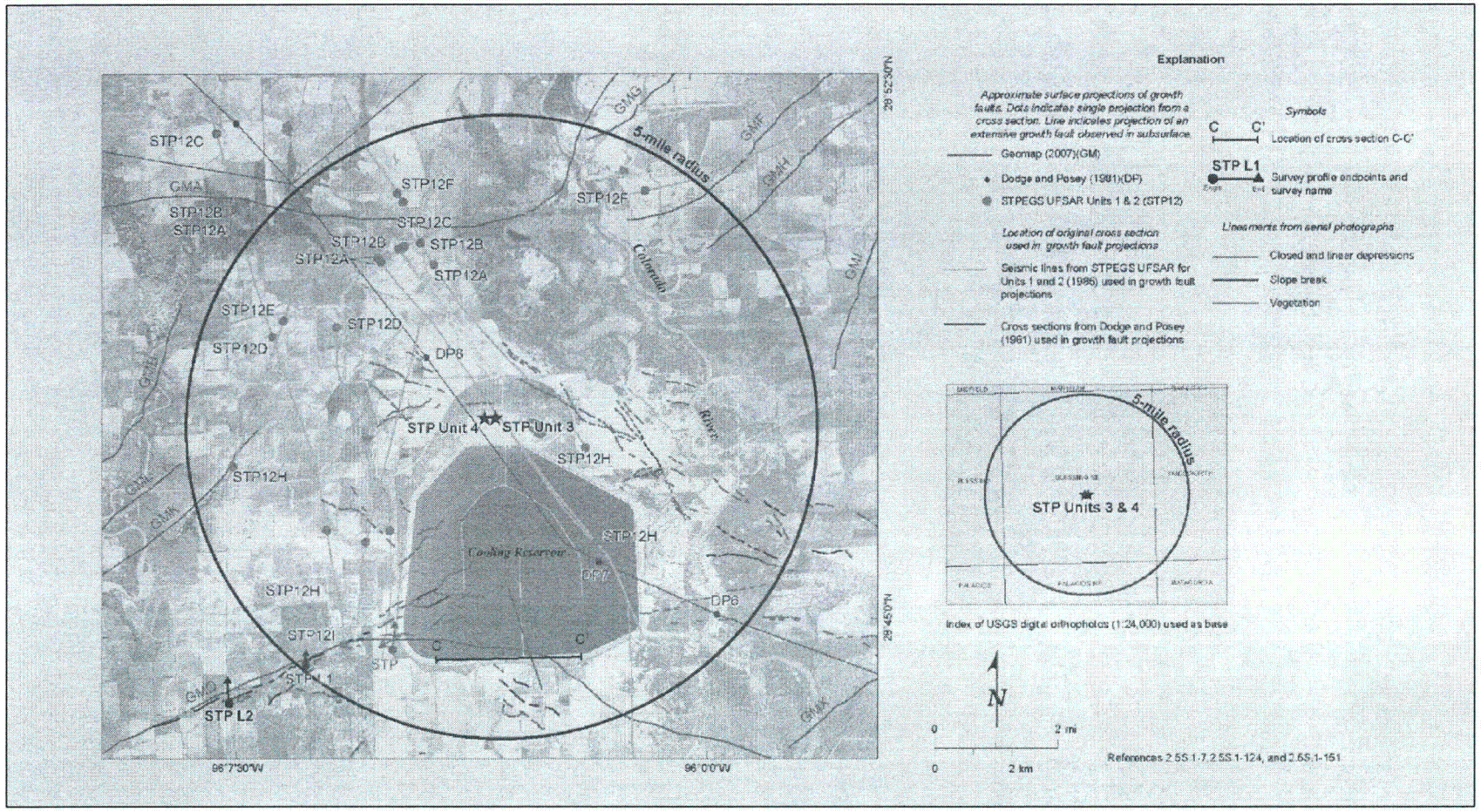

Figure 2.5S.1-45 Growth Fault Projections and Lineaments
[Previous version]

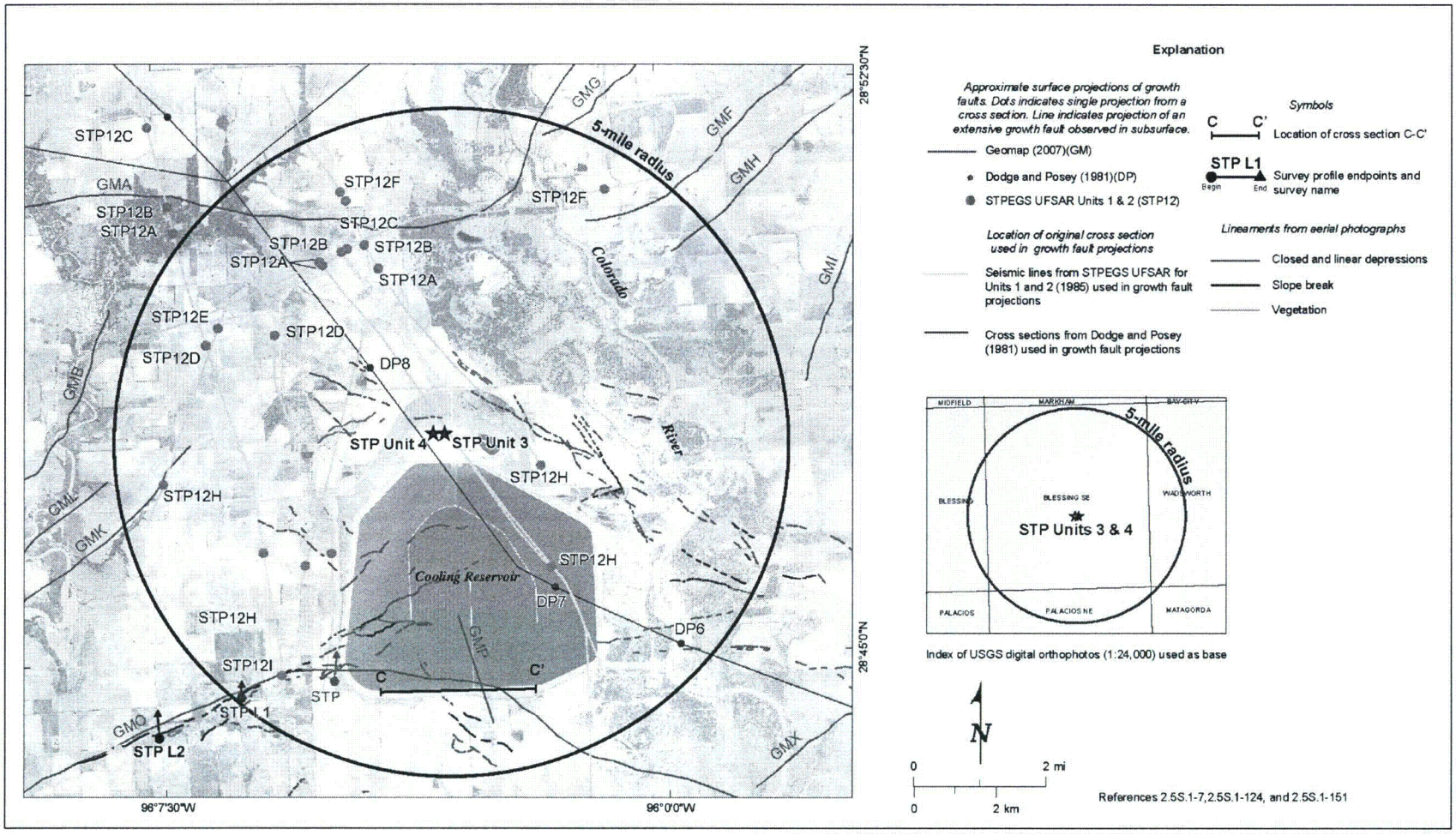

Figure 2.5S.1-45 Growth Fault Projections and Lineaments [New version]

RAI 02.05.02-11:

QUESTION:

Section 2.5S.2.4.1 describes seismic sources used from Bechtel Earth Science Team to calibrate its software and modeling parameters in trying to reproduce the 1989 EPRI results. You indicated that the results of this comparison are different depending on the EPRI ESTs. Therefore, listing only the Bechtel calibration results in Table 2.5 S.2-14 does not validate the calibration. Please provide detailed calibration results for the validation process.

RESPONSE:

Tables 252-11A through 252-11F show comparisons between EPRI-SOG hazards and hazards calculated during the validation process, for the Bechtel, Dames & Moore, Law Engineering, Rondout, Weston Geophysical, and Woodward-Clyde teams, respectively. These comparisons are for peak ground acceleration (PGA) amplitudes of 100, 250, and 500 cm/s2. Comparisons are made for the mean hazard and for the 15th, 50th, and 85th fractile hazards.

For the Rondout and Woodward-Clyde teams the comparisons are close except for the 15th fractile hazards, where the current hazards are much lower than the EPRI-SOG hazards. For these teams the host source was assigned a maximum magnitude (mmax) distribution that extended below mb 5.0 (with weights of 20% and 17% for the Rondout and Woodward-Clyde teams, respectively). Thus it is credible that the 15th fractile hazard would be very low, as currently calculated. The higher hazard reported in the EPRI-SOG study for the 15th fractile is attributed to undocumented assumptions in the EPRI-SOG analysis regarding mmax values for the Rondout and Woodward-Clyde sources.

For the Law team, the host source #126 has all values of mmax less than 5.0, and an adjacent source #124 (about 100 km distant) has an mmax distribution that extends below 5.0. Thus the current calculations indicate very low hazards, but the EPRI-SOG results are higher by several orders of magnitude. This difference is attributed to undocumented assumptions in the EPRI-SOG analysis regarding mmax values in the Law sources.

The Dames & Moore team used a "no-smoothing" assumption for the seismicity parameters in its sources 20, 25, and C08, and a lack of historical seismicity meant that no seismicity parameters were estimated in the degree cells near the site. In the current calculation, surrogate seismicity parameters were inserted in these degree cells that estimated rates equal to one-half the rates of adjacent cells. This gave mean and fractile hazards comparable to those reported by the EPRI-SOG study, except for the 85th fractile hazard which was over-estimated by 40-45%. This difference is attributed to undocumented assumptions in the EPRI-SOG analysis.

The other two teams, Bechtel and Weston, showed a good comparison between EPRI-SOG hazards and those currently calculated.

Table 252-11A: Hazard comparison, Bechtel team

PGA Amps		EPRI-SOG	Current Results	% difference
cm/s^2	Hazard			
100	mean	1.19E-05	1.20E-05	0.8%
	15%	4.22E-06	4.27E-06	1.2%
	50%	9.09E-06	9.12E-06	0.3%
	85%	1.82E-05	1.82E-05	0.0%
250	mean	1.35E-06	1.36E-06	0.7%
	15%	4.62E-07	4.68E-07	1.3%
	50%	9.58E-07	9.33E-07	-2.6%
	85%	2.28E-06	2.29E-06	0.4%
500	mean	1.30E-07	1.34E-07	3.1%
	15%	3.08E-08	3.16E-08	2.6%
	50%	8.87E-08	9.55E-08	7.7%
	85%	2.23E-07	2.34E-07	4.9%

Table 252-11B: Hazard comparison, Dames & Moore team

PGA Amps		EPRI-SOG	Current Results	% difference
cm/s^2	Hazard			
100	mean	9.52E-06	9.49E-06	-0.3%
	15%	2.13E-06	2.14E-06	0.5%
	50%	5.03E-06	5.25E-06	4.4%
	85%	1.02E-05	1.43E-05	40.2%
250	mean	1.21E-06	1.22E-06	0.8%
	15%	1.66E-07	1.66E-07	0.0%
	50%	4.50E-07	4.68E-07	4.0%
	85%	1.70E-06	2.46E-06	44.7%
500	mean	1.70E-07	1.74E-07	2.4%
	15%	6.64E-09	6.92E-09	4.2%
	50%	2.42E-08	2.75E-08	13.6%
	85%	2.92E-07	4.22E-07	44.5%

Table 252-11C: Hazard comparison, Law team

PGA Amps		EPRI-SOG	Current Results	% difference
cm/s^2	Hazard			
100	mean	1.13E-07	3.83E-09	-96.6%
	15%	1.19E-10	6.76E-29	-100.0%
	50%	1.20E-07	2.24E-11	-100.0%
	85%	2.09E-07	1.05E-08	-95.0%
250	mean	7.38E-09	2.87E-12	-100.0%
	15%	1.19E-10	6.76E-29	-100.0%
	50%	8.80E-09	2.34E-16	-100.0%
	85%	1.22E-08	3.47E-12	-100.0%
500	mean	2.69E-10	1.86E-15	-100.0%
	15%	1.19E-10	6.76E-29	-100.0%
	50%	4.18E-10	6.76E-29	-100.0%
	85%	5.20E-10	3.09E-16	-100.0%

Table 252-11D: Hazard comparison, Rondout team

PGA Amps		EPRI-SOG	Current Results	% difference
cm/s^2	Hazard			
100	mean	1.25E-05	1.25E-05	0.0%
	15%	4.44E-07	6.76E-29	-100.0%
	50%	1.26E-05	1.29E-05	2.4%
	85%	2.43E-05	2.40E-05	-1.2%
250	mean	1.22E-06	1.23E-06	0.8%
	15%	2.67E-08	6.76E-29	-100.0%
	50%	1.25E-06	1.32E-06	5.6%
	85%	2.18E-06	2.14E-06	-1.8%
500	mean	8.77E-08	9.18E-08	4.7%
	15%	9.87E-10	6.76E-29	-100.0%
	50%	8.18E-08	8.91E-08	8.9%
	85%	1.89E-07	1.66E-07	-12.2%

Table 252-11E: Hazard comparison, Weston team

PGA Amps		EPRI-SOG	Current Results	% difference
cm/s^2	Hazard			
100	mean	1.95E-05	1.96E-05	0.5%
	15%	6.86E-06	6.92E-06	0.9%
	50%	1.23E-05	1.29E-05	4.9%
	85%	2.74E-05	2.75E-05	0.4%
250	mean	2.02E-06	2.05E-06	1.5%
	15%	5.89E-07	5.75E-07	-2.4%
	50%	1.44E-06	1.41E-06	-2.1%
	85%	3.43E-06	3.47E-06	1.2%
500	mean	1.68E-07	1.75E-07	4.2%
	15%	2.64E-08	2.75E-08	4.2%
	50%	9.35E-08	1.02E-07	9.1%
	85%	3.50E-07	3.80E-07	8.6%

Table 252-11F: Hazard comparison, Woodward-Clyde team

PGA Amps		EPRI-SOG	Current Results	% difference
cm/s^2	Hazard			
100	mean	2.24E-05	2.25E-05	0.4%
	15%	3.49E-07	2.40E-29	-100.0%
	50%	1.35E-05	1.38E-05	2.2%
	85%	4.63E-05	4.79E-05	3.5%
250	mean	2.80E-06	2.82E-06	0.7%
	15%	2.92E-08	2.40E-29	-100.0%
	50%	1.32E-06	1.41E-06	6.8%
	85%	5.80E-06	5.62E-06	-3.1%
500	mean	3.39E-07	3.46E-07	2.1%
	15%	1.29E-09	2.40E-29	-100.0%
	50%	7.81E-08	8.91E-08	14.1%
	85%	6.69E-07	6.61E-07	-1.2%

No COLA revision is required as a result of this RAI response.

RAI 02.05.04-9:

QUESTION:

Section 2.5S.4.2.1.6 discusses Stratum F and the soil properties derived from field testing. Stratum F is predominantly a clay soil with a high percentage of fines and plasticity. The overall USCS classification of the soil is CH and CL. You corrected the SPT N-values to account for the overburden pressure and also to estimate undrained shear strength. However, you developed SPT overburden pressure corrections from large scale tests on granular soils (not clay soils). Please justify correcting N-values for CH and CL soils for all clay strata where N-values were corrected for the effects of overburden, considering that when N-values are corrected for overburden pressures less than 1 tsf, the corrected N-value would become unconservative (such as Stratum D).

RESPONSE:

As noted in the question, the N-values of not only the granular layers but also the cohesive layers were corrected for overburden pressure, using a correction factor developed for granular soils. This overburden correction for N-values of cohesive soils was considered to be a conservative approach, since it reduced the measured N-value for all soils located below about the mid-point of Stratum C, i.e., it reduced the N-values for all of the cohesive strata except Stratum A. For Stratum D, the overburden correction factor ranges from 0.85 at the top of the layer to 0.68 at the bottom of the layer. Thus, for Stratum D, correcting for overburden is conservative. For Stratum F, the correction factor ranges from 0.58 at the top of the layer to 0.51 at the bottom of the layer, and is 0.55 at mid-layer. This means that, at mid-layer, the measured N-value is reduced from 22 to 12 due to the overburden correction factor. Thus, application of the overburden correction factor to Stratum F is quite conservative. (Note that the measured N-values were also corrected for hammer energy to obtain the $(N_1)_{60}$ values used in the FSAR.)

The corrected N-values were taken into account when estimating the undrained shear strength (s_u) of cohesive layers, as shown on FSAR Table 2.5S.4-9. In all strata except Stratum A, the s_u value derived from the $(N_1)_{60}$ value was significantly less than the s_u value selected for design, which included consideration of s_u obtained from other sources (laboratory strength testing and cone penetration test (CPT) correlations). Thus, s_u derived from the N-values (except for Stratum A) had little impact on the s_u values selected for design. For Stratum A, where the overburden correction increased the measured N-value, the s_u value selected for design was less than the s_u value based on the N-value. Thus, for Stratum A, the increase in N-value due to the overburden correction was not reflected in the s_u value selected for design.

In summary, the overburden correction factors applied to the clay resulted in reduced (and thus conservative) N-values for all layers except Stratum A. The laboratory strength testing and CPTs were the primary data that were used for assigning design s_u values for the clay layers. The s_u values derived from the N-values for these layers had little to no impact on the s_u values selected for design. For Stratum A, the increase in N-value due to the overburden correction was not reflected in the s_u value selected for design and thus had no impact.

No COLA revision is required as a result of this RAI response.

RAI 02.05.04-10:

QUESTION:

Section 2.5S.4.2.1.6 discusses the Stratum F shear strength derivation. You assumed an undrained shear strength of 3.4 ksf to represent the layer based on the results of CPT testing and confirmed by higher shear strength values obtained in Stratum F at Units 1 and 2. Using an uncorrected average SPT N-value of 22, the undrained shear strength for stratum F determined from equation 2.5S.4-2 is 2.75 ksf, which agrees very well with the average results obtained from unconfined and UU testing (2.7 ksf). Please clarify how CPT shear strength correlations are more credible than laboratory test measurements, since you derived the site-specific cone factor from the laboratory test results.

RESPONSE:

For Stratum F, undrained shear strength values derived from SPT, CPT and laboratory strength tests from the STP 3&4 subsurface investigation were used to select a design undrained shear strength. In addition, laboratory strength results from STP 1&2 were also taken into account. The undrained shear strength values from these various sources are discussed below.

SPT N-Value

As noted in Section 2.5S.4.2.1.6, the average uncorrected N-value for Stratum F is 23 for the Unit 3 area and 22 for the Unit 4 area. All of the SPTs for STP 3&4 were obtained using automatic hammers. For the 11 rigs/hammers used, the energy ratio (ER) ranged from 1.21 to 1.65, as shown on Table 2.5S.4-4, with a median of 1.38 and an average of 1.39. Using the minimum ER of 1.21, the N-values corrected for hammer energy are 27.8 blows/ft for Unit 3 and 26.6 blows/ft for Unit 4. Using the median ER of 1.38, the N-values corrected for hammer energy are 31.7 blows/ft for Unit 3 and 30.4 blows/ft for Unit 4.

The overburden correction factor for N-value that was applied for Stratum F was derived from tests of granular materials. For deep strata (like Stratum F) it is conservative to apply this overburden correction factor to clay soils. However, there is no evidence that applying the overburden correction factor to clays is justified. If no overburden correction factor is applied, the undrained shear strength estimates obtained from equation 2.5S.4-2 are 3.4 ksf using the minimum ER and 3.9 ksf using the median ER. (The values for Unit 3 and Unit 4 were averaged in both cases.)

CPT Tip Resistance

The undrained shear strength of clays was estimated from CPT tip resistance using equation 2.5S.4-3 where the tip resistance minus the overburden pressure is divided by a factor N_{kt}. Reference 2.5.S.4-15 indicates that N_{kt} typically varies from 10 to 20, with 15 as an average. To estimate undrained shear strength for Stratum F from the STP 3&4 CPT results, a conservative value of $N_{kt} = 19$ was used. (This value correlated with laboratory measured strengths at a

limited number of locations.) If the average N_{kt} value of 15 had been used, the estimated undrained shear strength would have been about 4.5 ksf.

Laboratory Strength Tests

Table 2.5S.4-10 gives the results of the 10 UU triaxial tests performed on samples from Stratum F (no unconfined compression tests were performed). Although the average strength from the 10 tests was 2.7 ksf, examination of the results shows that majority of the tests gave strengths over 3 ksf. The median undrained shear strength from the 10 tests is 3.3 ksf. The median value is a more realistic value to use in this case since it reduces the influence of the 3 low results that were most probably the result of sample disturbance. As noted in Section 2.5S.4.2.1.6, the average undrained shear strength obtained from 23 UU triaxial tests performed on samples from Stratum F for STP 1&2 was about 4.8 ksf.

Summary

The values of undrained shear strength of the Stratum F clay discussed above are summarized in the following table.

Method	Undrained shear strength, ksf	Assumptions made
SPT using equation 2.5S.4-2	2.7	Uncorrected SPT N-value
	3.4	N corrected for minimum ER
	3.9	N corrected for median ER
CPT using equation 2.5S.4-3	3.6	$N_{kt} = 19$
	4.5	$N_{kt} = 15$
UU triaxial compression tests	2.7	Average of 10 UU tests
	3.3	Median of 10 UU tests
	4.8	Average of 23 STP 1&2 tests

The 3.4 ksf design value selected is reasonable based on the results from SPTs and UU triaxial testing listed above. The results from the CPTs are higher than the 3.4 ksf value. The CPT produces less soil disturbance than the SPT, and considerably less disturbance than the process to obtain samples for laboratory testing, especially at depths close to 100 ft, as in Stratum F. Thus the higher CPT results may more realistically reflect the in-situ strength of the Stratum F clay.

No COLA revision is required as a result of this RAI response.

RAI 02.05.04-11:

QUESTION:

Section 2.5S.4.2.1.6 describes the determination of the drained strength parameters for Stratum F. Drained strength parameters from CIU bar tests were effective phi = 8 degrees and effective cohesion = 2.0 tsf. This appears reasonable for an overconsolidated soil that was not tested at pressures above the preconsolidation pressure. However, in lieu of using data derived from Stratum F, the test assumed an effective phi of 20 degrees determined from testing stratum D for the analyses. Please clarify what makes stratum D test data more representative than Stratum F test data.

RESPONSE:

The effective cohesion (c') value for Stratum F tabulated in Section 2.5S.4.2.1.6 is incorrect. The value should be 2 ksf, not 2 tsf. The correct value of 2 ksf is given in the text immediately before the table. The same error occurs in the Stratum D and Stratum J (Clay) tabulated values for effective cohesion, i.e., tsf is used instead of ksf. These errors will be corrected.

The use of the effective phi (φ') of 20 degrees needs to be clarified. As noted by the reviewer, the average values of c' and φ' given in Section 2.5S.4.2.1.6 for Stratum F, i.e., c' = 2 ksf and φ' = 8°, appear to be reasonable values. The $\varphi' = 20°$ value was used only to compute the active, passive and at-rest earth pressure coefficients shown in Table 2.5S.4-16. Neglecting the effective cohesion of 2 ksf provides a conservative estimate of these coefficients, even though φ' was increased from 8° to 20°. The 20° value is derived from Table 1 of Reference 2.5S.4-13, as noted for Stratum A in Section 2.5S.4.2.1.1.

This clarification will be incorporated into the COLA. In Table 2.5S.4-16, the effective strength parameters for Stratum F, namely c' = 2 ksf and $\varphi' = 8°$ will replace $\varphi' = 20°$. There will be a footnote to the table indicating that $\varphi' = 20°$ is conservatively used for computing lateral earth pressure coefficients. Table 2.5S.4-16 will be similarly modified for Strata D and J (Clay). The text beneath the tabulated values of c' and φ' for Strata D, F and J (Clay) in Sections 2.5S.4.2.1.4, 2.5S.4.2.1.6, and 2.5S.4.2.1.8, respectively, will be modified to indicate that $\varphi' = 20°$ is conservatively used for computing lateral earth pressure coefficients.

COLA revisions are required as a result of this RAI response.

The tenth paragraph of Subsection 2.5S.4.2.1.4 Stratum D will be revised as follows:

> The drained friction angle of Stratum D soils was evaluated from laboratory test results. The results are shown in Table 2.5S.4-10 and summarized below. Strength parameters from two CIU-bar tests, indicated average (drained/effective) φ'=16 degrees, and c'=1.3 ksf, and average (undrained/total) φ=4 degrees and c=1.8 ksf, as noted:

Parameter	From CIU-Bar
φ' (degrees)	16
c' ~~(tsf)~~(ksf)	1.3
φ (degrees)	4
c ~~(tsf)~~(ksf)	1.8

~~Based on the above, a~~Note that φ'=20 degrees was ~~selected for Stratum D soils, and for similar fine-grained soil strata (i.e., Strata A, F, and J Clay).~~used to provide conservative values when computing lateral earth pressures.

The tenth paragraph of 2.5S.4.2.1.6 Stratum F will be revised as follows:

The drained friction angle of Stratum F soils was evaluated from laboratory test results. The results are shown in Table 2.5S.4-10 and summarized below. Strength parameters from three CIU-bar tests, indicated average (drained/effective) φ'=8 degrees and c'=2 ksf, and average (undrained/total) φ=3 degrees and c=2.1 ksf.

Parameter	From CIU-Bar
φ' (degrees)	8
c' ~~(tsf)~~(ksf)	2.0
φ (degrees)	3
c ~~(tsf)~~(ksf)	2.1

~~Based on the results of CIU-bar tests made on Stratum D (having similar plasticity to Strata A, F, and J Clay, as noted above),~~Note that φ'=20 degrees was ~~selected for Stratum F soils.~~used to provide conservative values when computing lateral earth pressures.

The seventh paragraph of 2.5S.4.2.1.8.1 Sub-stratum J Clay will be revised as follows:

The drained friction angle of Sub-Strata J Clay soils was evaluated from laboratory test results. The results are shown in Table 2.5S.4-10 and summarized below. Strength parameters from seven CIU-bar tests, indicated average (drained/effective) φ'=8 degrees and c'=2.6 ksf and average (undrained/total) φ=4 degrees and c=2.9 ksf.

Parameter	From CIU-Bar
φ' (degrees)	8
c' ~~(tsf)~~(ksf)	2.6
φ (degrees)	4
c ~~(tsf)~~(ksf)	2.9

~~Based on the results of CIU-bar tests made on Stratum D (having similar plasticity to Strata A, F, and J Clay, as noted above),~~Note that φ'=20 degrees was

~~selected for Sub-stratum J Clay soils~~ used to provide conservative values when computing lateral earth pressures.

The first and second tables of Table 2.5S.4-16 Summary of Average Geotechnical Engineering Parameters will be revised as follows on the next pages:

Table 2.5S.4-16 Summary of Average Geotechnical Engineering Parameters

	Stratum				
Parameter [1]	**A/A (Fill)**	**B**	**C**	**D**	**E**
Average Thickness, feet	18	7	20	22	18
USCS Group Symbol	CH, CL	ML, CL, SM	SM, SP-SM	CH, CL	SP-SM, SM
Natural Moisture content (MC), %	23	24	24	25	21
Moist Unit Weight, (moist), pcf	124	121	122	121	122
Fines content, %	94	71	25	72	18
Liquid Limit (LL), %	57	38	N/A	58	N/A
Plasticity Index (PI), %	37	19	N/A	38	N/A
Uncorrected SPT N-value, bpf	10	9	24	15	35
Corrected SPT (N1)60-value, bpf	15	10	35	15	30
Shear Wave Velocity (Vs), feet/sec	575	725	785	925	1,080
Undrained shear strength (sU), ksf	1.6	N/A	N/A	3.0	N/A
Drained Friction Angle (Ø'), degrees	N/A	30	35	~~2016~~ [2]	35
Drained Cohesion, (c'), ksf	N/A	N/A	N/A	~~N/A1 3~~ [2]	N/A
Elastic modulus (High Strain) (Es), ksf	1,050	460	850	2,500	1,100
Shear modulus (High Strain) (Gs), ksf	360	185	320	850	425
Shear modulus (Low Strain) (Gmax), ksf	1,270	1,970	2,740	3,210	4,420
Coefficient of Subgrade Reaction (k1), kcf	150	160	600	300	600
Earth Pressure Coefficients					
-Active (Ka)	0.5	0.3	0.3	0.5	0.3
- Passive (Kp)	2.0	3.0	3.7	2.0	3.7
-At-rest (K0)	0.7	0.5	0.4	0.7	0.4
Sliding Coefficient (tangent)	0.30	0.35	0.40	0.30	0.40
Consolidation Properties					
-Compression Index (Cc)	0.235	N/A	N/A	0.255	N/A
-Recompression Index (Cr)	0.017	N/A	N/A	0.023	N/A
-Preconsolidation Pressure (Pc'), ksf	6.3	N/A	N/A	12.3	N/A
-Overconsolidation Ratio (OCR)	7.0	N/A	N/A	3.3	N/A

[1] The values tabulated above are guidelines. Reference should be made to the specific boring log, CPT log, and laboratory test results for appropriate modifications at specific locations and/or for specific calculations

[2] Values of φ'=20 degrees and c' = 0 are used to provide conservative values when computing lateral earth pressures.

Table 2.5S.4-16 Summary of Average Geotechnical Engineering Parameters (Continued)

Parameter [1]	Stratum F	H	J Clay	J Sand	K Clay
Average Thickness, feet	16	17.5	61 [2]	37.5 [3]	18.5
USCS Group Symbol	CH, CL	SP-SM, SM	CH	SM, ML	CL
Natural Moisture content (MC), %	24	19	23	23	20
Moist Unit Weight, (moist), pcf	125	128	125	125	129
Fines content, %	89	16	89	43	75
Liquid Limit (LL), %	58	N/A	54	N/A	39
Plasticity Index (PI), %	38	N/A	35	N/A	25
Uncorrected SPT N-value, bpf	22	44	31	65	15
Corrected SPT (N1)60-value, bpf	15	30	15	35	6
Shear Wave Velocity (Vs), feet/sec	945	1,075	1,145	1,275	1,145
Undrained shear strength (sU), ksf	3.2	N/A	3.5	N/A	3.0
Drained Friction Angle (Ø'), degrees	~~208~~ [4]	35	~~208~~ [4]	33	N/A
Drained Cohesion, (c'), ksf	~~N/A2.0~~ [4]	N/A	~~02.6~~ [4]	N/A	N/A
Elastic modulus (High Strain) (Es), ksf	2,600	1,150	3,500	1,500	3,100
Shear modulus (High Strain) (Gs), ksf	900	450	1,200	600	1,050
Shear modulus (Low Strain) (Gmax), ksf	3,470	4,590	5,090	6,310	5,480
Coefficient of Subgrade Reaction (k1), kcf	300	600	N/A	N/A	N/A
Earth Pressure Coefficients					
-Active (Ka)	0.5	0.3	N/A	N/A	N/A
- Passive (Kp)	2.0	3.7	N/A	N/A	N/A
-At-rest (K0)	0.7	0.4	N/A	N/A	N/A
Sliding Coefficient (tangent)	0.30	0.40	N/A	N/A	N/A
Consolidation Properties					
-Compression Index (Cc)	0.240	N/A	0.228	N/A	0.176
-Recompression Index (Cr)	0.039	N/A	0.040	N/A	0.017
-Preconsolidation Pressure (Pc'), ksf	15.5	N/A	18.5	N/A	18.3
-Overconsolidation Ratio (OCR)	2.6	N/A	1.7	N/A	1.3

[1] The values tabulated above are guidelines. Reference should be made to the specific boring log, CPT log, and laboratory test results for appropriate modifications at specific locations and/or for specific calculations

[2] Sub-stratum J Clay thickness = combined thickness of J Clay 1 (29 feet) + J Clay 2 (32 feet) 37.5

[3] Sub-stratum J Sand thickness = combined thickness of J Interbed 1 (9 feet) + J Sand 1 (13.5 feet)+ J Interbed 2 (15 feet)

[4] Values of $\varphi' = 20$ degrees and $c' = 0$ are used to provide conservative values when computing lateral earth pressures.